J Physiol 00.0 (2018) pp 1–23

The Journal of Physiology

Metabolic remodelling of glucose, fatty acid and redox pathways in the heart of type 2 diabetic mice

Sonia Cortassa[1], Viviane Caceres[2,3], Carlo G. Tocchetti[2,4], Michel Bernier[5], Rafael de Cabo[5], Nazareno Paolocci[2,6], Steven J. Sollott[1] and Miguel A. Aon[1,5]

[1] *Laboratory of Cardiovascular Science, National Institute on Aging/NIH, Baltimore, MD 21224, USA*
[2] *Division of Cardiology, Department of Medicine, The Johns Hopkins University, Baltimore, MD 21205, USA*
[3] *Posgraduate Program in Rehabilitation Sciences, Dept. Health Sciences, Federal University of Santa Catarina, Ararangua, SC, Brazil*
[4] *Dipartimento di Scienze Mediche Traslazionali, Universita' degli Studi di Napoli Federico II Via Pansini 5, Edificio 2, 80131 Napoli, Italy*
[5] *Translational Gerontology Branch, National Institute on Aging/NIH, Baltimore, MD 21224, USA*
[6] *Department of Biomedical Sciences, University of Padova, via Marzolo 3, 35131, Padova, Italy*

Edited by: Don Bers & Satoshi Matsuoka

Key points

- Hearts from type 2 diabetic animals display perturbations in excitation–contraction coupling, impairing myocyte contractility and delaying relaxation, along with altered substrate consumption patterns.
- Under high glucose and β-adrenergic stimulation conditions, palmitate can, at least in part, offset left ventricle (LV) dysfunction in hearts from diabetic mice, improving contractility and relaxation while restoring coronary perfusion pressure.
- Fluxome calculations of central catabolism in diabetic hearts show that, in the presence of palmitate, there is a metabolic remodelling involving tricarboxylic acid cycle, polyol and pentose phosphate pathways, leading to improved redox balance in cytoplasmic and mitochondrial compartments.
- Under high glucose and increased energy demand, the metabolic/fluxomic redirection leading to restored redox balance imparted by palmitate helps explain maintained LV function and may contribute to designing novel therapeutic approaches to prevent cardiac dysfunction in diabetic patients.

Abstract Type-2 diabetes (T2DM) leads to reduced myocardial performance, and eventually heart failure. Excessive accumulation of lipids and glucose is central to T2DM cardiomyopathy. Previous data showed that palmitate (Palm) or glutathione preserved heart mitochondrial energy/redox balance under excess glucose, rescuing β-adrenergic-stimulated cardiac excitation–contraction coupling. However, the mechanisms underlying the accompanying improved contractile performance have been largely ignored. Herein we explore in intact heart under

Sonia Cortassa has a PhD in Chemical Sciences from the Universidad Nacional de Córdoba, Argentina, and has held research and teaching positions at Universidad Nacional de Tucumán and Consejo Nacional Investigaciones Científicas y Técnicas (CONICET). In the USA, she has continued her research at the Johns Hopkins University and, at present, at the Laboratory of Cardiovascular Science/National Institute on Aging/NIH. Her field of research is Physiology, Bioenergetics, with expertise in Computational modelling of metabolic networks. She believes that quantitative Systems Biology approaches represent a real opportunity to contribute to the understanding of human body function in health and disease.

DOI: 10.1113/JP276824

substrate excess the metabolic remodelling associated with cardiac function in diabetic *db*/*db* mice subjected to stress given by β-adrenergic stimulation with isoproterenol and high glucose compared to their non-diabetic controls (+/+, WT) under euglycaemic conditions. When perfused with Palm, T2DM hearts exhibited improved contractility/relaxation compared to WT, accompanied by extensive metabolic remodelling as demonstrated by metabolomics–fluxomics combined with bioinformatics and computational modelling. The T2DM heart metabolome showed significant differences in the abundance of metabolites in pathways related to glucose, lipids and redox metabolism. Using a validated computational model of heart's central catabolism, comprising glucose and fatty acid (FA) oxidation in cytoplasmic and mitochondrial compartments, we estimated that fluxes through glucose degradation pathways are ~2-fold lower in heart from T2DM *vs.* WT under all conditions studied. Palm addition elicits improvement of the redox status via enhanced β-oxidation and decreased glucose uptake, leading to flux-redirection away from redox-consuming pathways (e.g. polyol) while maintaining the flux through redox-generating pathways together with glucose–FA 'shared fuelling' of oxidative phosphorylation. Thus, available FAs such as Palm may help improve function via enhanced redox balance in T2DM hearts during peaks of hyperglycaemia and increased workload.

(Received 13 July 2018; accepted after revision 15 November 2018; first published online 21 November 2018)
Corresponding author S. Cortassa: Laboratory of Cardiovascular Science, National Institute on Aging/NIH, Baltimore, MD 21224, USA. Email: sonia.cortassa@nih.gov

Introduction

Type 2 diabetes (T2DM) is a disorder that leads to extensive metabolic remodelling, with both elevated glucose and elevated fatty acids (FAs). The T2DM heart relies more prominently on FA utilization than healthy hearts (Boudina & Abel, 2010), and this shift in substrate utilization could be a major driver of the cardiac dysfunction that is a key hallmark of the T2DM syndrome. In fact, the negative feedback exerted by FA utilization on glycolysis via the so-called Randle mechanism (Randle *et al.* 1963; Hue & Taegtmeyer, 2009) has been proposed as a key contributor to impaired ATP supply and increased reactive oxygen species (ROS) emission from the heart (Anderson *et al.* 2009; Boudina & Abel, 2010). However, when FA utilization is reduced/altered, hyperglycaemia *per se* becomes a major factor of excessive ROS production, leading to myocardial tissue structural and thus functional alterations (Williamson *et al.* 1993; Brownlee, 2001).

We previously observed that exposing isolated T2DM (*db*/*db*) myocytes (or hearts) to β-adrenergic stimulation together with isoproterenol (ISO), to mimic exercise, and to high glucose (HG), to simulate peaks of hyperglycaemia as in the case of poor glycaemic control, prompts marked perturbations in excitation–contraction (EC) coupling, impairing myocyte contractility and delaying relaxation (Tocchetti *et al.* 2012). These observations were later confirmed in a type 1 diabetic model (streptozotocin-treated guinea pigs) (Tocchetti *et al.* 2015), or heart trabeculae from T2DM Zucker diabetic fatty rat (Bhatt *et al.* 2015). Of note, exogenous glutathione (GSH) or, even more so, the fatty acid palmitate (Palm), rescued function in *db*/*db* myocyte/heart preparations exposed to HG/ISO by restoring the reducing equivalents necessary to counter T2DM-related excess mitochondrial ROS production and energetic failure (Tocchetti *et al.* 2012). Yet how a redirection in cardiac metabolic fluxes restores the myocardial redox balance, together with function, in T2DM hearts remains unclear.

Systems biology computational methods have been pivotal to addressing the integrated functional dynamics of metabolic, organelle and cellular networks (Kurz *et al.* 2017). Metabolic disorders, cancer and caloric restriction, which have an impact on lifespan (Mitchell *et al.* 2016), together with pharmacological interventions able to modulate redox metabolism and healthspan (Mitchell *et al.* 2018), are conspicuous examples of data-driven research that can directly benefit from quantitative knowledge of physiological and molecular mechanisms underlying their respective systemic states. Cardiac function is constantly changing in response to energy demand (Cortassa *et al.* 2006; Zhou *et al.* 2009, 2014; Goh *et al.* 2016). Hence, a systems biology approach should be ideal to better understand how, during T2DM, changes in metabolic fluxes alter myocardial redox conditions and function. Previous studies have, for instance, assessed the relevance of pathways such as the polyol (Vikramadithyan *et al.* 2005; Giacco & Brownlee, 2010), pentose phosphate (Jain *et al.* 2003; Hecker *et al.* 2013*b*), glycolytic or glycogenolytic (Kashiwaya *et al.* 1994; Goodwin *et al.* 1998) pathway on heart or vascular (endothelial) function, each taken separately. Yet a quantitative metabolomics–fluxomics approach, flanked by computational modelling and bioinformatics analyses, is still lacking *de facto*, precluding a more integrative

evaluation of heart's glucose and FA catabolism in T2DM preparations.

Here we designed and performed experiments to address this knowledge gap, using intact, Langendorff-perfused hearts from diabetic (*db*/*db*) mice and their non-diabetic (+/+) controls (WT) exposed to substrate conditions mimicking their corresponding circulation levels of glucose and Palm, alone or in combination with ISO, in the presence or absence of Palm, to determine how metabolic fluxes in WT *vs.* *db*/*db* mice are redirected, and whether, and to what extent, these eventual metabolic/flux shifts can be reversed by Palm. To investigate this, we evaluated the unloaded heart contractile performance alongside bioinformatic analysis of metabolite profiling combined with computational kinetic modelling of glucose and FA utilization pathways.

Table 1. Study design for metabolite profiling in Langendorff-perfused intact heart from WT and *db*/*db* mice

Group	*n*	Description
WT-G	6	WT mouse, perfusion glucose 11 mM
WT-GI	6	WT mouse, perfusion glucose 11 mM/ISO 10 nM
WT-GIP	6	WT mouse, perfusion glucose 11 mM/ISO 10 nM/Palm 0.2 mM
db-G	6	*db*/*db* mouse, perfusion glucose 30 mM
db-GI	6	*db*/*db* mouse, perfusion glucose 30 mM/ISO 10 nM
db-GIP	6	*db*/*db* mouse, perfusion glucose 30 mM/ISO 10 nM/Palm 0.4 mM

Global biochemical profiles were obtained from whole heart tissue derived from WT or *db*/*db* mice perfused with glucose (G), glucose + isoproterenol (GI), or glucose + ISO + Palm (GIP) as indicated (see Methods).

Table 2. Glucose and fatty acid concentrations in plasma of WT and *db*/*db* mice

Plasma levels	WT	*db*/*db*	Reference
Glucose (mM)	12.2 ± 0.5	29.1 ± 0.7	Tocchetti *et al.* (2012)
Fatty acids (mEq L^{-1})	1.1 ± 0.3	1.5 ± 0.3	The Jackson Laboratory monitoring[a]
Palmitate (mM)	0.22–0.28	0.3–0.38	Wisneski *et al.* (1987); Balogun *et al.* (2013)

[a]https://www.jax.org/jax-mice-and-services/solutions-by-therapeutic-area/metabolic-diseases/featured-mice-for-type-2-and-obesity/phenotype-information-for-000642
Glucose, mean ± SEM; Fatty acids, mean ± SD; Palmitate, mean ± SD

Methods

Ethical approval

Male C57BLKS/J-*leprdb*/*leprdb* diabetic (*db*/*db*) and non-diabetic C57BLKS/J-*lepr*+/*lepr*+ (+/+) (WT) mice, 8–10 weeks of age (Tocchetti *et al.* 2012), were obtained from The Jackson Laboratory (Bar Harbor, ME, USA). Mice were euthanized with an intraperitoneal pentobarbital-based solution (100 mg kg^{-1} I.P.) following the procedures established by the Institutional Animal Care/Use Committee at Johns Hopkins University, adhering to NIH guidelines. Ethical approval documentation has been provided to *The Journal of Physiology* Editorial Office.

Preparation and perfusion of mouse hearts

Following rapid excision after euthanasia, *db*/*db* or WT hearts were retrogradely perfused (Langendorff technique) according to the protocol described in Table 1. Briefly, *db*/*db* or WT hearts were retrogradely perfused (Langendorff technique) with Krebs–Henseleit buffer, pH 7.4, containing (in mM): 1.2 P_i, 0.5 free Mg^{2+}, 1.07 free Ca^{2+} and 11 glucose for ∼30 min. After stabilization, the perfusion was switched to one of three buffer solutions containing (i) glucose (G, 11 mM for WT or 30 mM for *db*/*db*), (ii) glucose plus 10 nM isoproterenol (ISO) (GI), or (iii) glucose+ISO+Palm (GIP) containing 0.2 mM (WT) or 0.4 mM Na-Palm (*db*/*db*), bound to fatty acid-free bovine serum albumin (ratio 4:1 lipid to protein) prepared as described (Tocchetti *et al.* 2012). Substrate concentrations were chosen to mimic circulating glucose and Palm levels under normal *in vivo* conditions in both groups, which were measured directly or estimated from C57BL mice data as shown in Table 2. Hearts were perfused during ∼30 min while monitoring left ventricle (LV) function and vascular tone through coronary perfusion pressure (CPP) under all conditions except for ISO addition, in which it remained for ∼10 min until maximal response to the β-agonist. Hearts were paced with a Radnoti pacing electrode (Monrovia, CA, USA) at 600 bpm (10 Hz, 4 ms duration, 4 V) using a Grass stimulator (Grass Instruments Co., Quincy, MA, USA). LV function was monitored with a water-filled, customized latex balloon connected to a P23XL pressure transducer with interface cable (Harvard Apparatus, Holliston, MA, USA) and coupled to a BIOPAC System (DA100, Santa Barbara, CA, USA) for continuous data recording and offline analysis. LV end-diastolic pressure was set at 5–10 mmHg by adjusting the balloon volume with a Gilmont micrometer syringe (Cole-Parmer, Vernon Hills, IL, USA).

Metabolite profiling

After perfusion, hearts were snap frozen in liquid nitrogen and sent to Metabolon, Inc. (Research Park Triangle, NC,

USA) for metabolite profiling. Untargeted metabolomics was performed as described before (Cortassa *et al.* 2015), detecting a total of 261 identifiable metabolites.

Bioinformatic analyses

MetaboAnalyst 3.0 (Xia *et al.* 2015), an integrated web-based platform for comprehensive analysis of metabolomic data (Xia & Wishart, 2011) was utilized. Univariate (ANOVA), clustering (heat map, correlation matrix) and multivariate (partial least square discriminant; PLSD) statistical analyses were applied to the metabolite profiles. According to PLSD analysis both genotypes exhibit good separation as a function of treatment, and a subset of 46 metabolites responsible for the separation were determined.

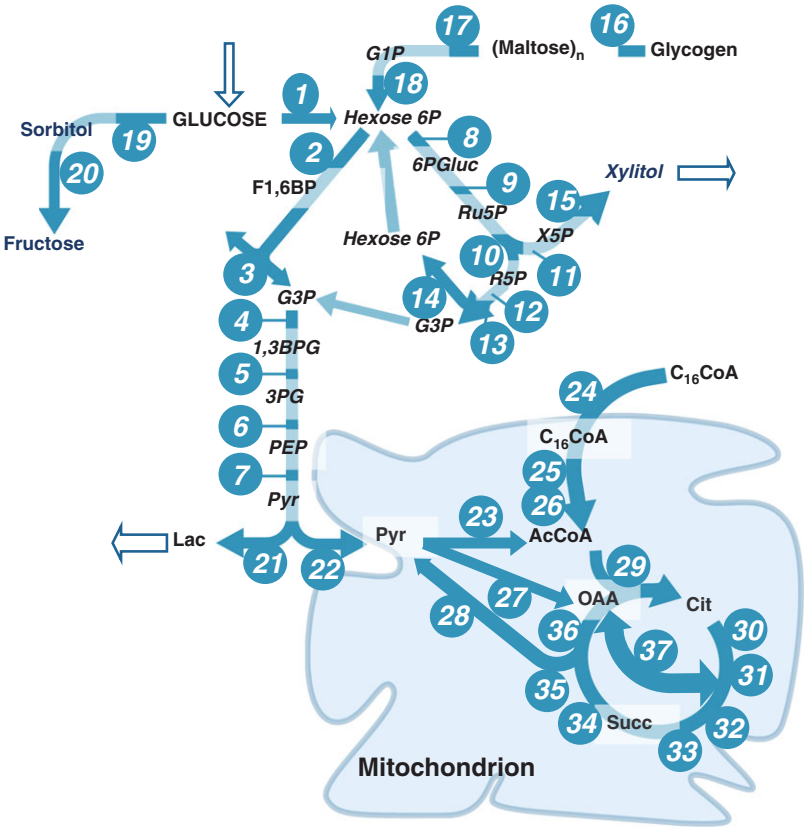

Figure 1. Scheme of the computational model of central catabolism used for metabolomics–fluxomics analysis
Depicted is a scheme of the model of central catabolism of oxidative pathways from glucose and FAs (Palm) in cytoplasmic and mitochondrial compartments. Open arrows indicate the exchange of the metabolite with the extracellular medium. Filled arrows indicate intracellular enzymes/processes. Enzymes: (1) HK, hexokinase; (2) PFK, phosphofructokinase; (3) ALD, aldolase; (4) GAPD, glyceraldehyde 3 phosphate dehydrogenase; (5) PGK, phosphoglycerol kinase; (6) Eno, enolase; (7) PK, pyruvate kinase; (8) G6PD, glucose 6 phosphate dehydrogenase; (9) 6 PGO, 6 phosphogluconate dehydrogenase; (10) R5PI, ribose 5P isomerase; (11) Ru5PE, ribulose 5P epimerase; (12) TK1, transketolase 1; (13) TAL, transaldolase; (14) TK2, transketolase 2; (15) XDH, xylitol dehydrogenase; (16) Gno_is, glycogen breakdown; (17) GPa,b, glycogen phosphorylase; (18) PGLM, phosphoglucomutase; (19) ALDR, aldose reductase; (20) SoDH, sorbitol dehydrogenase; (21) LDH, lactate dehydrogenase; (22) PyrT, pyruvate carrier; (23) PDH, pyruvate dehydrogenase; (24) CPT1, carnitine palmitoyl transferase 1; (25) CAD, fatty acyl CoA dehydrogenase; (26) bMTP, beta-oxidation multienzyme complex; (27) PyrCb, pyruvate carboxylase; (28) ME, malic enzyme; (29) CS, citrate synthase; (30) Aco, aconitase; (31) IDH, isocitrate dehydrogenase; (32) aKGDH, alpha-ketoglutarate dehydrogenase; (33) SL, succinyl CoA lyase; (34) SDH, succinate dehydrogenase; (35) FH, fumarase; (36) MDH, malate dehydrogenase; (37) AAT, aspartate amino transferase. Metabolites: 1,3BPG, 1,3-bisphosphoglycerate; 3PG, 3-phosphoglycerate; 6PGluc, 6-phosphogluconate; AcCoA, acetyl-CoA; C_{16}CoA, palmitoyl-CoA; Cit, citrate; F1,6BP, fructose 1,6-bisphosphate; G1P, glucose 1-phosphate; G3P, glyceraldehyde 3-phosphate; hexose-6P, accounts for glucose 6-phosphate plus fructose 6-phosphate; Lac, lactate; (Maltose)*n*, maltooligosaccharides (maltose, malto-triose, -tetraose, -hexaose, etc.); OAA, oxaloacetate; PEP, phosphoenolpyruvate; Pyr, pyruvate; R5P, ribose 5-phosphate; Ru5P, ribulose 5-phosphate; Succ, succinate; X5P, xylulose 5-phosphate. [Colour figure can be viewed at wileyonlinelibrary.com]

For selected metabolites, two-way ANOVA (Prism 7.0, GraphPad Software, San Diego, CA, USA) was performed with Sidak's multicomparison test for two groups (genotypes: WT, *db*/*db*) and three treatments (G, GI, GIP). The statistical significance of the effect of genotype, treatment and their interaction was evaluated for selected metabolites from central catabolism showing that their level was influenced by both genotype and treatment whereas only a few of them exhibited significant interaction between genotype and treatment.

From metabolomics to fluxomics: general methodological description

The procedure to translate metabolomics into fluxomics was described in detail elsewhere (Cortassa *et al.* 2015). In the present work, we extend our methodology to account for main catabolic pathways (glucose and FAs), including cytoplasmic and mitochondrial processes. We also consider mitochondrial membrane substrate carriers (pyruvate and carnitine palmitoyltransferase 1) along with pyruvate dehydrogenase, including its main regulators.

Computational modelling of central catabolism

A detailed computational kinetic model of the glucose and FAs utilization pathways was built according to the scheme shown in Fig. 1. Previously we have described the rate expressions of the kinetic model for each enzymatic step of glucose catabolism (glycolysis, glycogenolysis, polyol, pentose phosphate (PP) pathways) and polyol transport (Cortassa *et al.* 2015), FA catabolism (β-oxidation, lipid transport) (Cortassa *et al.* 2017*a*) as well as the link between them via mitochondrial pyruvate transport and

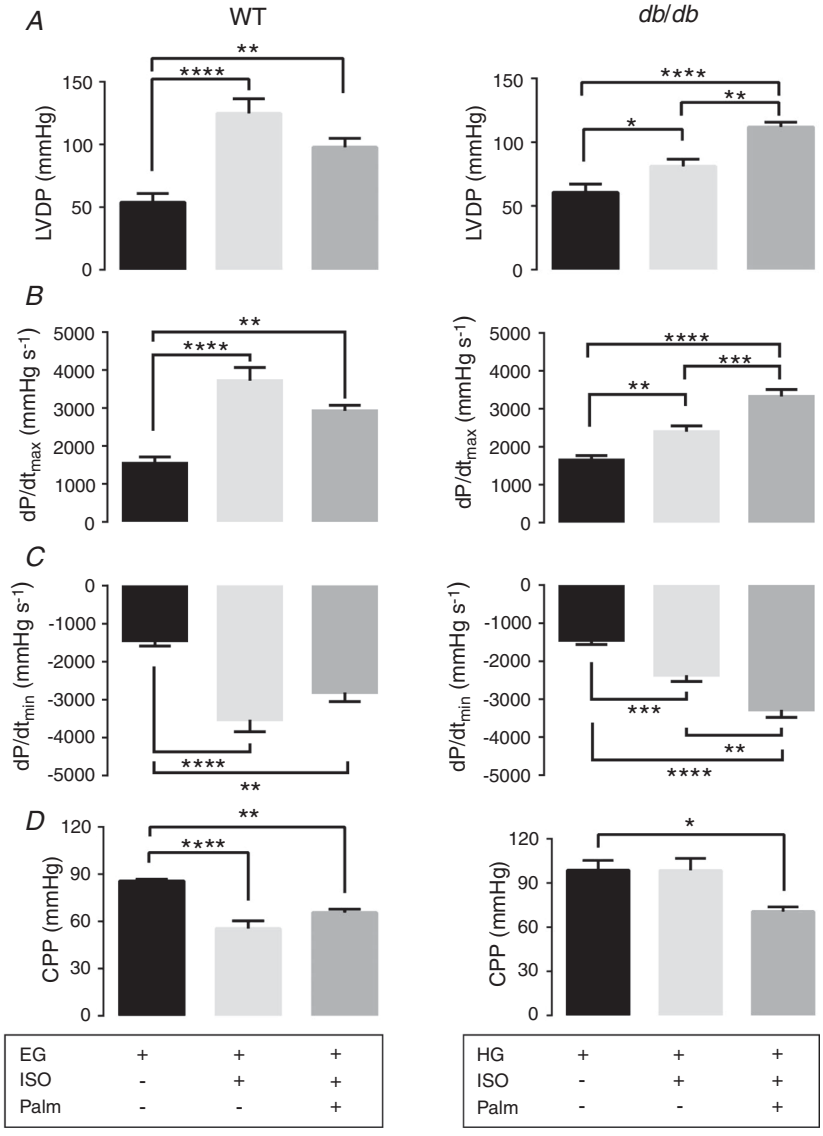

Figure 2. Vascular tone and LV function in Langendorff-perfused WT and *db*/*db* mouse hearts
Mouse hearts were harvested, handled and perfused as described (Tocchetti *et al.* 2012). Shown are the LVDP (*A*), CPP (*D*) (both in mmHg), and maximal rates of contraction (dP/dt_{max}) (*B*) and relaxation (dP/dt_{min}) (*C*) (both in mmHg s^{-1}). The data presented correspond to $n = 18$ hearts in each group of WT or *db*/*db*, and $n = 6$ for each treatment, i.e. G, GI, GIP. $^{*}P < 0.05$; $^{**}P < 0.01$; $^{***}P < 0.001$; $^{****}P < 0.0001$.

pyruvate dehydrogenase (Cortassa *et al.* 2017*b*) integrated to other mitochondrial energetic-redox processes (Wei *et al.* 2011; Kembro *et al.* 2013). The model equations, both differential equations and rate expressions, are detailed in the Supporting information.

In all cases, the rate equations consider the effect of known regulatory interactions and effectors, among many, e.g. ATP for glucose 6-phosphate dehydrogenase (G6PD), AMP and citrate for phosphofructokinase (PFK) (Cortassa *et al.* 2009, 2017*a*), multiple effectors (acetyl-CoA (AcCoA), CoA, NADH, NAD, ATP, ADP, Ca^{2+}, pyruvate) that regulate the pyruvate dehydrogenase complex via dedicated kinase(s) and phosphatase(s), which phosphorylate (inactivating) or dephosphorylate (activating), respectively, the enzymatic complex (Cortassa *et al.* 2017*b*).

Kinetic modelling of metabolic networks

Computer model simulations as a function of time or analysed at the steady state were carried out with MATLAB (The MathWorks, Natick, MA, USA). The kinetic model of glucose catabolism is represented by a system of ordinary differential equations (ODEs S1–S34: Supporting information) which was computed as a function of time until a steady state was reached, i.e. when the state variables derivative is less than 1×10^{-10}. The MATLAB built-in solver ODE15s, designed for stiff equations, was used as integrator.

Linear optimization of V_{max} in the kinetic model

The V_{max} of each enzyme is the only unknown kinetic parameter subjected to optimization. Metabolic enzymes may change their amounts following transcriptional–translational regulation, or their activity after post-translational modifications, which are reflected by their V_{max} values. For optimization, we represented the rate of each step in the metabolic network by explicit rate expressions which are, in all cases, a linear function of V_{max}. The latter assumption is required for applying linear optimization methods. To calculate V_{max} values, the optimization of the linear algebraic system was performed using the MATLAB linprog function with the 'Simplex' algorithm. Maximization of ATP synthesis fluxes or minimization of redox consumption were used as objective functions to constrain the optimization procedure.

In addition to metabolite concentrations, reference fluxes are needed for V_{max} optimization. Reference fluxes were provided by the rates of exchange of metabolites with the extracellular medium, such as rates of glucose and FA consumption, and lactate efflux. Glucose and FA consumption rates were estimated from the rates determined for cardiomyocytes, evaluated in a Seahorse XFe96 extracellular flux analyser accounting for oxygen consumption and lactic acid efflux when either glucose or Palm was the substrate. The rates of substrate consumption determined in cardiomyocytes were scaled to match the rate of oxygen consumption determined by Boardman *et al.* (2009) in unloaded hearts.

Fluxome calculation

Within the volume of possible solutions, the one chosen fulfilled the following two conditions: (i) $V_{max} > 0$ for all enzyme activities in the network, and (ii) belongs to the edge of the hypervolume (solution space) of the metabolic network (Cortassa *et al.* 2015, 2018). With the solution at hand, i.e. the set of optimized V_{max} values, we ran computer simulations to reproduce the initial metabolite profile. The fluxes through each individual step of the metabolic network, obtained by dynamic simulations at the steady state, correspond to the 'fluxome'.

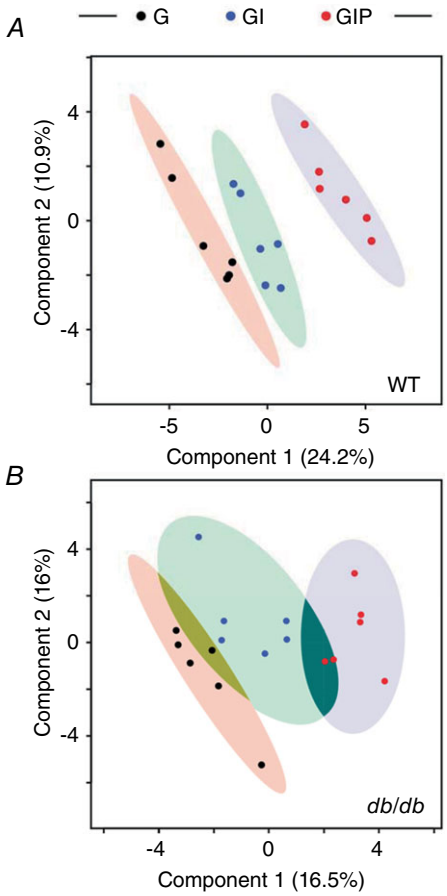

Figure 3. Partial least square discriminant (PLSD) analysis of WT and diabetic heart metabolomes
PLSD analysis is a cross-validated multivariate supervised clustering/classification method from MetaboAnalyst that we used to determine the extent of separation afforded by a subset of 43 metabolites that exhibited significant changes in response to different treatments (G, GI, GIP) within each group (WT, *db/db*).

Results

LV function and coronary vasodilation in WT and *db*/*db* hearts challenged with high glucose and β-adrenergic stimulation

Exposing isolated T2DM (*db*/*db*) myocytes (or hearts) to β-AR stimulation with ISO and HG – to simulate peaks of hyperglycaemia as per poor glycaemic control and neurohormonal stimulation, respectively – prompts marked perturbations in the EC coupling process, negatively affecting myocyte contractility and delaying relaxation (Tocchetti *et al.* 2012).

Here, we first aimed at corroborating these findings while obtaining perfused heart tissue to perform metabolomic–fluxomic analysis to determine which glucose and FA catabolic pathways are modified in *db*/*db* *vs.* WT mice, in the absence or presence of HG or ISO, or both. Moreover, since we previously showed that Palm prevents loss in LV function in T2DM myocytes/hearts treated with HG+ISO (Tocchetti *et al.* 2012), we next compared the impact of Palm on these hearts *vs.* WT hearts perfused with the *in vivo* circulating levels of glucose (i.e. 11 mM WT and 30 mM *db*/*db*) + ISO to determine whether Palm differentially affects LV function and fluxomics/metabolomics in WT *vs.* *db*/*db* hearts.

Consistent with previous reports (Boudina *et al.* 2007; Tocchetti *et al.* 2012), Palm decreased ISO-evoked enhancement in LV function in euglycaemic WT hearts. Although this effect was manifest in terms of developed pressure (LV-developed pressure; LVDP; Fig. 2*A*), dP/dt_{max} (Fig. 2*B*) and dP/dt_{min} (Fig. 2*C*), the decline in cardiac performance elicited by Palm in the WT did not reach statistical significance for any of the variables measured. Of note, coronary perfusion pressure (CPP, Fig. 2*D*) declined similarly in ISO-treated WT hearts, regardless of the presence or absence of Palm. Thus, under euglycaemic conditions, Palm addition alters ISO's ability to enhance myocardial function, but it does not affect ISO-induced coronary vasorelaxation.

In *db*/*db* hearts without Palm, the β-agonist-evoked enhancement of contractility/relaxation (Fig. 2*A*–*C*) was markedly blunted while ISO's ability to reduce coronary vascular tone was countered (Fig. 2*D*). Controls for WT and *db*/*db* hearts in the presence of corresponding

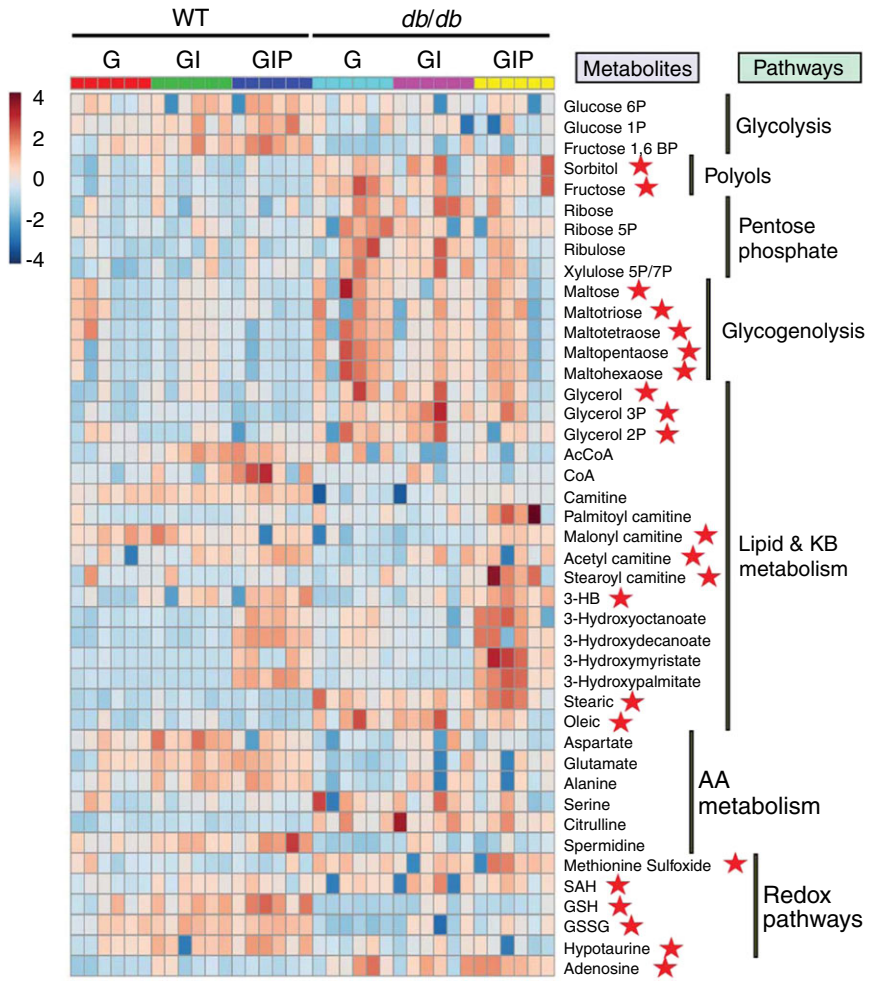

Figure 4. Heat map of significantly changed metabolites in the heart metabolomes from WT and diabetic mice
The relative abundance of intermediates from different pathways in WT and *db*/*db* hearts is displayed under the different experimental conditions assayed, as described in the legends of Fig. 2 and Table 1. Depicted is the heat map of the normalized levels of 43 metabolites mainly responsible for the separation between groups (WT, *db*/*db*) and treatments (G, GI, GIP) (see Fig. 3) from central glucose and FA degradation pathways, along with redox-related pathways such as methionine cycle and transsulfuration routes. The heat map was constructed using the web-based resource MetaboAnalyst 3.0 (Xia & Wishart, 2016). Graded pseudo-colours brown and blue correspond to metabolites accumulation or depletion, respectively, according to the scale placed at the left of the plot. AA, amino acid; GSH, reduced glutathione; GSSG, oxidized glutathione; 3-HB, 3-hydroxybutyrate; KB, ketone body; SAH, S-adenosylhomocysteine.

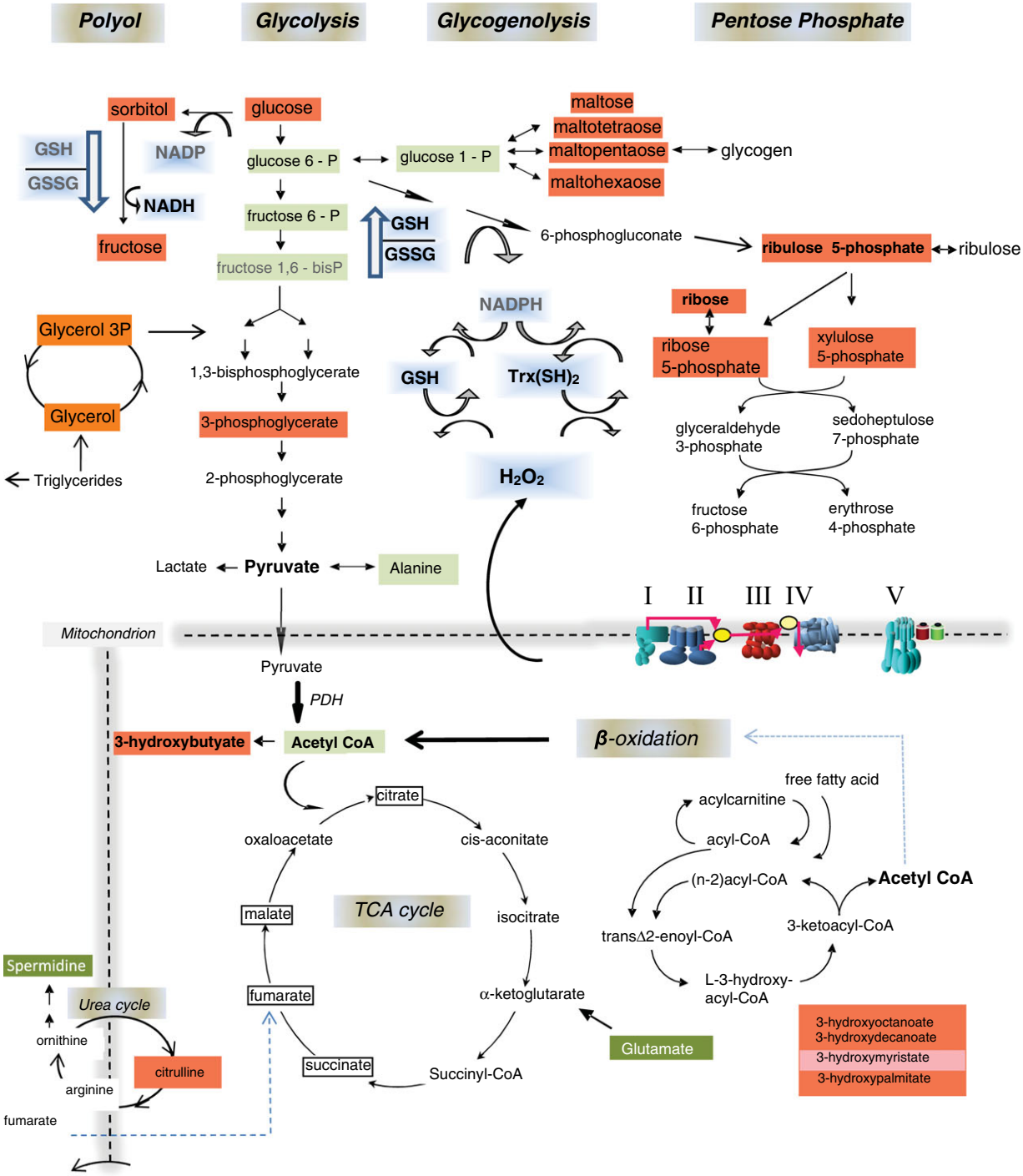

Figure 5. Cytoplasmic and mitochondrial main metabolic routes of glucose and FA catabolism in WT and *db*/*db* hearts
Displayed are glucose and FA degradation pathways, including the urea cycle (highlighted blue) in both cytoplasmic and mitochondrial compartments. Also present in the scheme is the impact of different pathways, e.g. polyol, pentose phosphate, TCA cycle, β-oxidation, on the redox status (NADPH, ROS). Depicted in red and green are the pathway location and relative levels of metabolites in diabetic *vs.* WT hearts subjected to the GIP condition. In *db*/*db* hearts subjected to GI, Palm addition elicited metabolite accumulation (red: $P < 0.05$) or depletion (green: $P < 0.05$) with respect to WT. The quantitative assessment of metabolite levels (in mM) is shown in Tables 3 and 4. GSH, reduced glutathione; GSSG, oxidized glutathione; Trx, thioredoxin; Trx(SH)2, reduced thioredoxin.

substrate combinations for euglycaemic and hyperglycaemic conditions were previously reported (Tocchetti *et al.* 2012). Unlike in WT, increased contractility and relaxation in *db*/*db* hearts were attained in the presence of Palm co-perfused with HG and ISO (Fig. 2*A*–*C*). Under the latter conditions, Palm addition also restored the coronary vascular response to ISO (Fig. 2*D*). Hence, this dataset confirms previous findings that Palm rescues LV function in *db*/*db* hearts challenged with HG+ISO, and suggesting that, in part, Palm's beneficial effects stem from ISO's preserved ability to decrease coronary regulatory vascular tone and flow to enable its better matching with ventricular muscle metabolic demands (see also Tocchetti *et al.* 2012, their Fig. 6 and Supplementary Figs S5–S7).

Heart metabolomics from WT and T2DM *db*/*db* mice

To address the metabolic mechanisms underlying the preserved contractile performance of the diabetic heart in response to β-adrenergic stimulation in the presence of excess glucose and lipid, we carried out a quantitative metabolomics–fluxomics approach flanked by computational modelling and bioinformatic analysis of the WT *vs.* T2DM (*db*/*db*) heart. To achieve this goal, untargeted metabolite profiling was performed in the same Langendorff-perfused WT and *db*/*db* hearts (as per Fig. 2). Metabolomics revealed a total of 261 metabolites, and combined univariate (two-way ANOVA) and multivariate (PLSD) analyses enabled us to obtain a subset of 43 metabolites that accounts for the separation of the metabolite profiles of G-, GI- and GIP-treated hearts, for both genotypes. Figure 3 shows the principal components, with component 1 on the *x*-axis explaining 24% and 16.5% of the 43 metabolites variance in WT and *db*/*db* mouse hearts, respectively, and component 2 on the *y*-axis accounting for 10.9% and 16% of the variance in WT and *db*/*db*, respectively (Fig. 3). This approach allows the separation between treatments within both

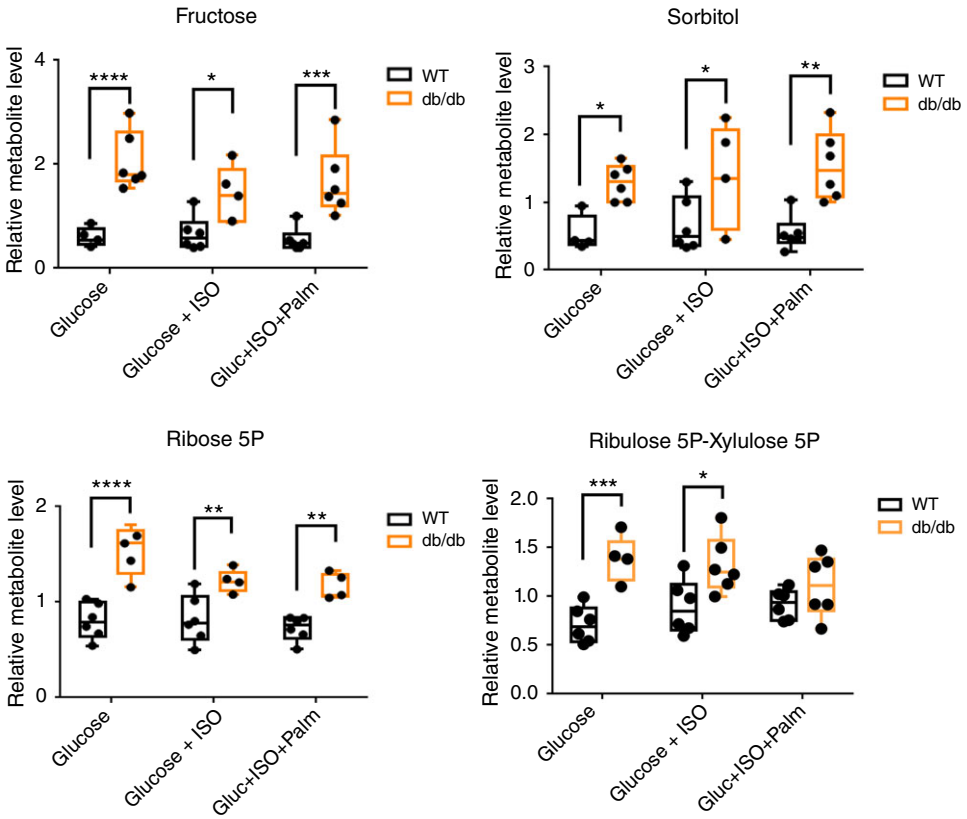

Figure 6. Two-way ANOVA of metabolites from polyol and pentose phosphate pathways
Displayed are whisker plots showing the normalized relative levels of metabolite intermediates of the polyol and pentose phosphate pathways from WT and *db*/*db* hearts. Significantly increased levels of sorbitol and fructose from polyol, and ribulose-5P, ribose, ribose-5P and xylulose-5P from the PP pathway were present in the metabolite profiles from *db*/*db* mice suggesting that both pathways are active. In excess glucose, especially in the presence of Palm, and high energy demand, the heart appears to be able to shunt glucose to polyol and PP pathways. Interestingly, the impact on the cardiac myocyte redox status would be opposite, i.e. polyol depletes NADPH while PP increases the level of this reducing equivalent (Fig. 5). Therefore, the degree activation of the PP respect to the polyol pathway will determine cytoplasmic redox. $^{*}P < 0.05$; $^{**}P < 0.01$; $^{***}P < 0.001$; $^{****}P < 0.0001$. [Colour figure can be viewed at wileyonlinelibrary.com]

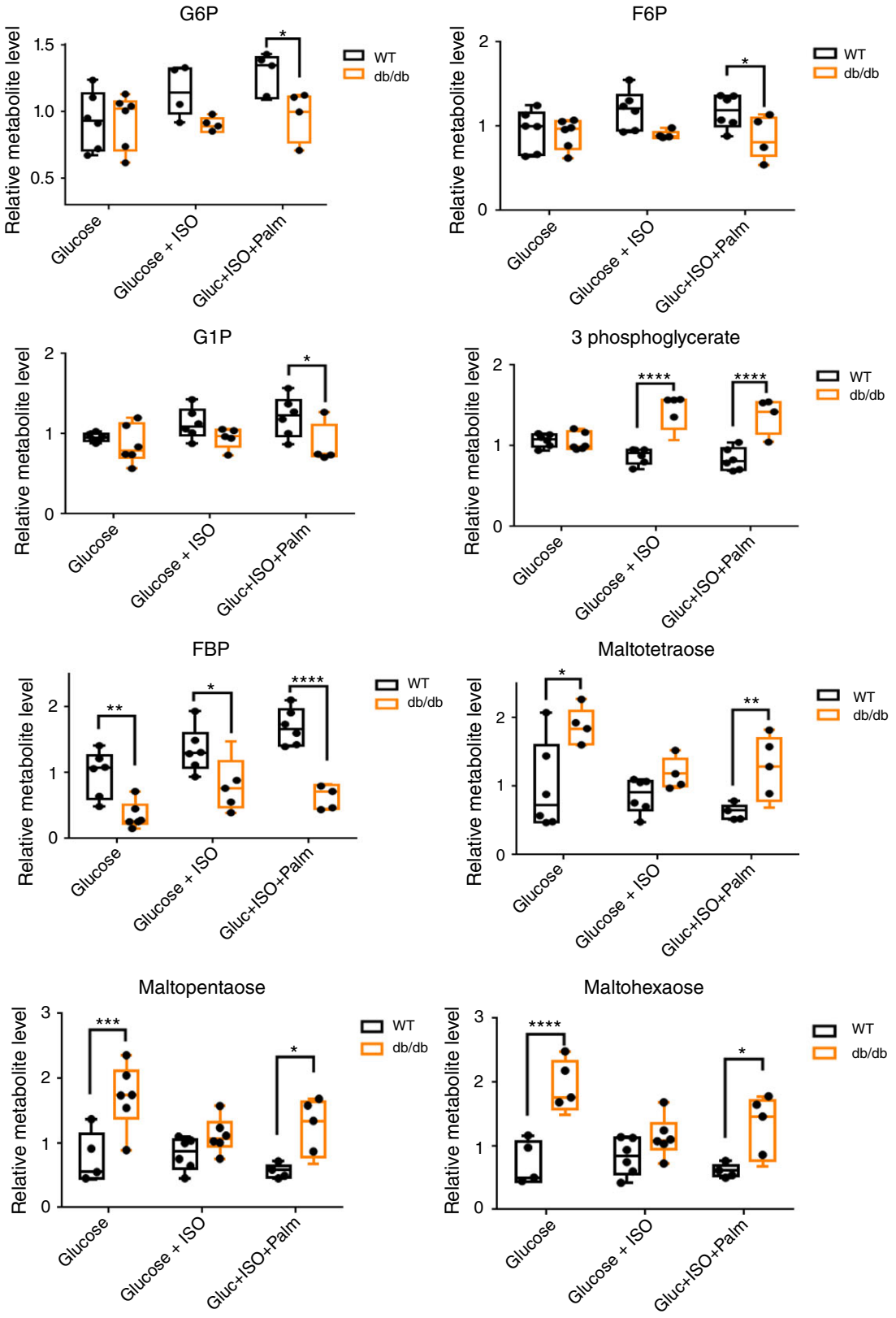

Figure 7. Two-way ANOVA of metabolite intermediates from glycolysis and glycogenolysis
Displayed are the whisker plots showing the normalized relative levels of metabolite intermediates from glycolytic and glycogenolytic pathways in WT and *db/db* hearts. Several metabolites from the upper part of glycolysis such as F6P, G6P and F1,6BP were significantly depleted in diabetic as compared to WT hearts, whereas downstream

groups, which are displayed with their corresponding 95% confidence regions. A heat map of the 43 main metabolites demonstrated the presence of clearly distinct patterns of relative abundance between WT and diabetic mice (Fig. 4). More specifically, significantly more abundant or depleted metabolites mapped into central catabolic pathways (Fig. 5) from glucose metabolism in hearts from diabetic mice with respect to WT. Our analysis revealed the presence of members of the polyol pathway, namely sorbitol and fructose, glycogenolysis (malto-oligosaccharides such as -tetraose and-pentaose), the non-oxidative branch of the PP pathways (i.e. ribose, ribose-5P, ribulose, xylulose-5P/7P) and of stearic and oleic fatty acid oxidation. In *db*/*db* mouse hearts, most intermediary metabolites belonging to these pathways were accumulated with respect to WT (Figs 4–7). In the presence of Palm, similar abundance of metabolites from FA oxidation (e.g. 3-hydroxymyristate, 3-hydroxydecanoate) in both strains (Fig. 4) together with relative depletion of the amino acids aspartate, glutamate and alanine, as well as the redox-energy biosynthetic carriers AcCoA and CoA, and of TCA cycle intermediates, in diabetic *vs.* WT, suggest anaplerotic replenishment of pyruvate and TCA cycle metabolite pool (Figs 4, 5, 8 and 9), which was concomitant with high mitochondrial metabolic fluxes (see below).

Other pathways, feeding into central catabolism, were also apparent in the metabolite profiles. In *db*/*db* hearts, the intermediates (glycerol, glycerol-3P) from the glycerol-3P/glycerol cycle were more abundant than in WT ones (Figs 4 and 5). The glycerol-3P/glycerol cycle, situated at the intersection of glucose and lipid metabolism, shunts glycerol away from triglyceride degradation into glycolysis (Fig. 5). Catalysed by phosphoglycolate phosphatase, the available glycerol-3P formed from dihydroxyacetone-P in glycolysis can be dephosphorylated to glycerol, thus functioning as a 'glycerol-3P phosphatase' (Mugabo *et al.* 2016). In this way, the glycerol pool from triglyceride degradation is enriched, and glycerol can then be exported or shuttled back to glycolysis, as recently proposed for heart metabolism (Possik *et al.* 2017).

Concerning the oxidative stress-prone conditions in *db*/*db* hearts, redox-related metabolism involving methionine cycle and transsulfuration pathways leading to glutathione synthesis exhibited relatively higher abundance in diabetic mice of methionine sulfoxide, a biomarker of oxidative stress. Together with the significant depletion of hypotaurine, and of the reduced (GSH) and oxidized (GSSG) forms of glutathione (Fig. 10), these findings suggest overwhelming of the methionine cycle and transsulfuration pathways, consistent with the enhanced oxidative stress exhibited by T2DM *db*/*db* mice (Tocchetti *et al.* 2012) and by Zucker rats (Bhatt *et al.* 2015). Aminothiol homocysteine from the transsulfuration pathway has been implicated as a biomarker of oxidative stress in patients exhibiting chronic heart failure (Causse *et al.* 2017), and shown to be involved in cardioprotection (Nakano *et al.* 2015).

An overview of the differences between the metabolic behaviour of WT and *db*/*db* mice is captured by the correlation matrix of the 43 main metabolites. Diabetic mouse heart showed a larger and different cluster of positively correlated metabolites than that of the WT. Within the large cluster, a subcluster of strongly positively correlated metabolites (Fig. 11, large and smaller brackets, respectively) comprising metabolites from glycogen degradation, PP, glycerol cycle, β-oxidation and lipid metabolism pathways, was apparent.

Thus, in the presence of excess glucose, the heart metabolome of diabetic mice exhibited clusters of positively correlated metabolites from several pathways of glucose metabolism with, in principle, opposing negative (polyol, transsulfuration) and positive (PP) effects on cellular redox as well as glucose/lipid utilization as revealed by glycerol-3P/glycerol cycle and β-oxidation metabolism enhancement.

Fluxome remodelling in the diabetic heart subjected to high energy demand in the presence of excess glucose and lipid

To quantify fluxes from glucose and Palm through the central catabolic pathways in the heart, we calculated the fluxome underpinning the alterations in metabolites' accumulation/depletion, as shown in Figs 4–9. Applying our metabolomic–fluxomic approach, first, we converted relative metabolite levels into concentrations, and, secondly, utilizing our computational kinetic model of central catabolism (Fig. 1) and analytical platform, we estimated metabolic fluxes as previously described (Cortassa *et al.* 2015).

As a validation step of the computational model, Tables 3 and 4 show the metabolites' concentration experimentally determined in *db*/*db* and WT hearts, respectively, compared with model simulations, under

in the same path, 3PG accumulated in a significant way in diabetic mice. Significant depletion of both G6P and G1P and accumulation of malto-oligosaccharides suggest predominant glycogen degradation. Together, this metabolite pattern indicates that when the heart is subjected to increased energy demand in the presence of excess glucose and Palm, glycolysis is fully functional and fed not only from external glucose but also from internal glycogen stores. $^{*}P < 0.05$; $^{**}P < 0.01$; $^{***}P < 0.001$; $^{****}P < 0.0001$. 3PG, 3-phosphoglycerate; F1,6BP, fructose 1,6-bisphosphate; F6P, fructose 6-phosphate; G1P, glucose 1-phosphate; G6P, glucose 6-phosphate. [Colour figure can be viewed at wileyonlinelibrary.com]

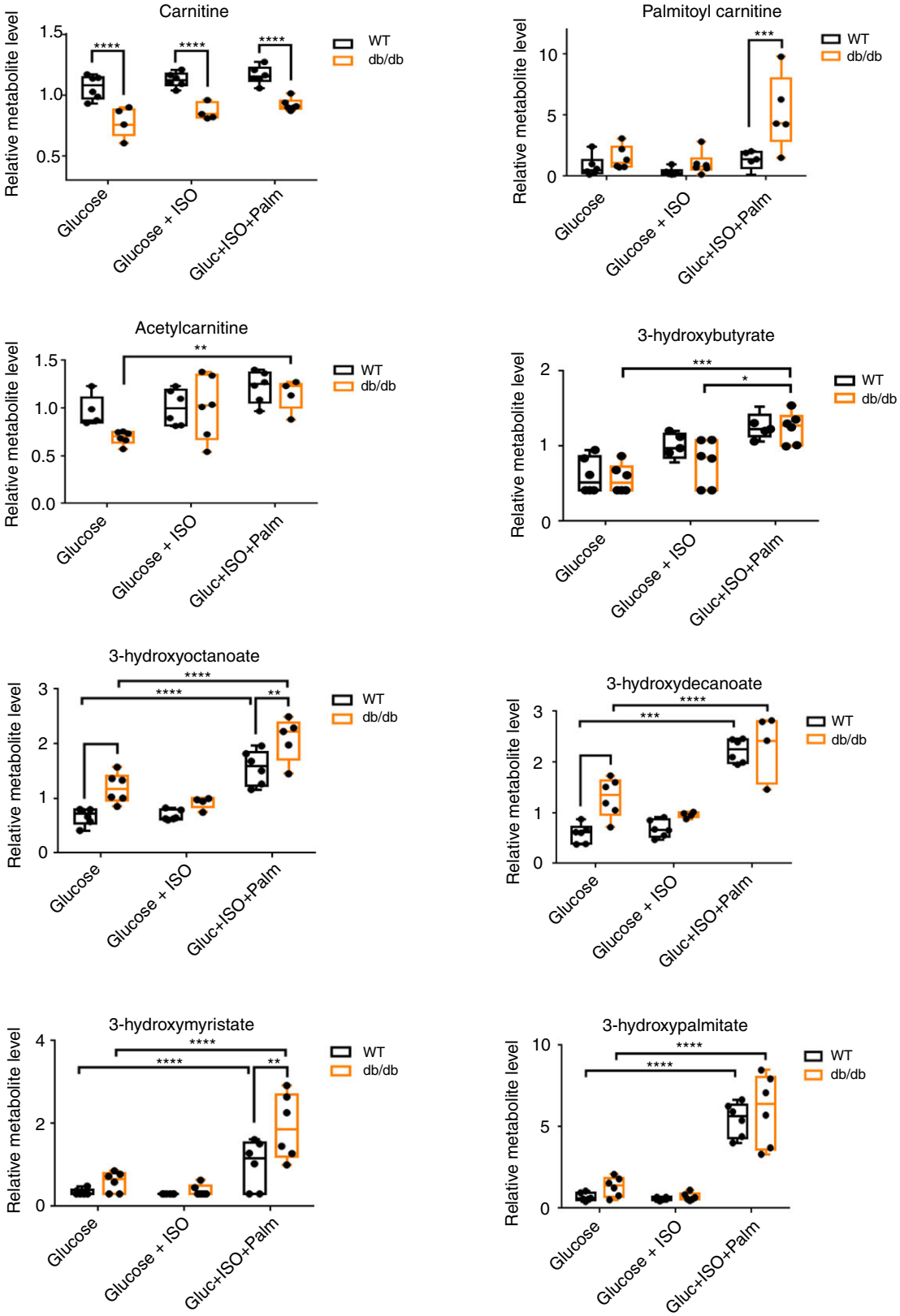

Figure 8. Two-way ANOVA of metabolites from fatty acid-oxidation
Expectedly, several intermediates from this pathway accumulated to significant levels in the presence of Palm in WT and diabetic hearts, although the levels of 3-hydroxyoctanoate and 3-hydroxymyristate were significantly

all experimental conditions. The computational model closely reproduces metabolite concentrations from the profiles observed experimentally (Tables 3 and 4).

Next, using the model and the metabolite concentrations, we determined the fluxome or set of metabolic fluxes that gives rise to the experimental metabolite concentration profile. We calculated the flux distribution through glucose and FA catabolism in cytoplasmic and mitochondrial compartments displayed by WT and *db*/*db* hearts perfused with glucose in the presence or absence of ISO and Palm.

Cytoplasmic fluxome in T2DM heart: favourable redox balance by decreased polyol contribution and preserved flux through the pentose phosphate pathway

The flux of glucose uptake in T2DM hearts perfused with HG was 20% lower than in WT, despite the approximately 3-fold glucose concentration difference in the perfusate (Fig. 12). Palm addition further decreased up to 20% the flux through glycolysis concomitant with a 17-fold decrease in the intracellular concentration of glucose compared to the G or GI condition (Tables 3 and 4). With lipid, the ratio of Palm oxidation over glucose uptake shifted from 0.024 to 0.026 in WT and from 0.032 to 0.0525 in T2DM, indicating that in the *db*/*db* heart the presence of lipid increases 64% its relative oxidation with respect to glucose.

The glucose fluxome immediately upstream and downstream of the branch leading to polyol, glycogenolysis or PP routes revealed that, regardless of the presence or absence of ISO and Palm, most fluxes in the *db*/*db* heart are 2- to 3-fold slower than in WT; for example, there is a 3-fold decrease, from 148 to 50 μM s^{-1}, in the flux of glycogen degradation from T2DM *vs.* WT heart (Fig. 12). The polyol pathway was a conspicuous exception since its flux was ∼5-fold higher in the diabetic heart in the absence of Palm; on the contrary, with Palm the polyol flux diminished ∼6-fold to WT level. Of note, however, is that the polyol pathway only represents 0.15–2% of the flux through glycolysis. Unlike the polyol pathway leading to sorbitol and fructose, the efflux of the polyol xylitol was ∼30% lower in the diabetic compared to WT heart. Interestingly, although in the *db*/*db* heart the glycolytic flux decreased 20% in the presence of Palm, the PP flux was maintained (Fig. 12).

Mitochondrial fluxome in T2DM heart: enhanced availability of reducing equivalents via increased FA oxidation and flux partitioning through the TCA cycle

There was a 10% higher FA oxidation flux in the diabetic group in the absence of Palm but 35% greater in its presence (Fig. 12, Palm uptake flux: 4.2 − 3.1 = 1.1 compared to 3.1) with respect to the WT, suggesting active oxidative mitochondrial metabolism, including via β-oxidation and the TCA cycle. Since the lipid energy content becomes available from β-oxidation as reducing equivalents and AcCoA of which the latter, after further processing in the TCA cycle, also supplies most of the energy as NADH and $FADH_2$, these results agree with the expected large requirement of reducing equivalents by the T2DM heart anticipated by previous work with diabetic rodents (Tocchetti *et al.* 2012; Bhatt *et al.* 2015).

In the mitochondrial matrix, the aspartate aminotransferase (AAT) reaction catalyses the reversible conversion of oxaloacetate (OAA) to α-ketoglutarate (αKG), dividing the TCA cycle both conceptually and functionally into 'upper' (αKG–OAA–citrate) and 'lower' (αKG–succinate–OAA) parts, in addition to the normal mode of cycling throughout (Fig. 12). Interestingly, AAT exhibits a *flux-direction change* between WT and T2DM hearts: (i) negative, involving the upper part, or (ii) positive, involving the lower part, of the TCA cycle, respectively (Fig. 12). When negative (WT heart), the flux through AAT involving the upper part represents ∼7% of the total flux through the TCA cycle, whereas in the diabetic heart it amounts to ∼17% of the total for the lower part. Notably, the redox outcomes, i.e. NADH generation, are different consisting of 1 NADH for the upper part *vs.* 2 NADH plus the electrons channelled to complex II in the respiratory chain via succinate dehydrogenation through the lower part.

Altogether, the results indicate the metabolic mechanisms underlying the improved redox status observed in the T2DM heart in the presence of Palm. The heart from diabetic mice subjected to HG in the absence of exogenous Palm, under all conditions assayed, exhibits overall ∼2-fold lower than WT fluxes through central catabolism from glucose, and only 10% higher from endogenous FAs. In the T2DM heart, the addition of Palm elicits a 20% flux reduction in both glucose uptake and glycolysis, concomitant with 17-fold decrease in intracellular glucose, and a 35% increase in FA oxidation flux with respect to WT heart.

higher in diabetic mice. Carnitine and palmitoyl carnitine were significantly decreased and increased, respectively, in diabetic hearts, which is also expected in the presence of increased mitochondrial β-oxidation when the heart is subjected to higher energy demand. *$P < 0.05$; **$P < 0.01$; ***$P < 0.001$; ****$P < 0.0001$. [Colour figure can be viewed at wileyonlinelibrary.com]

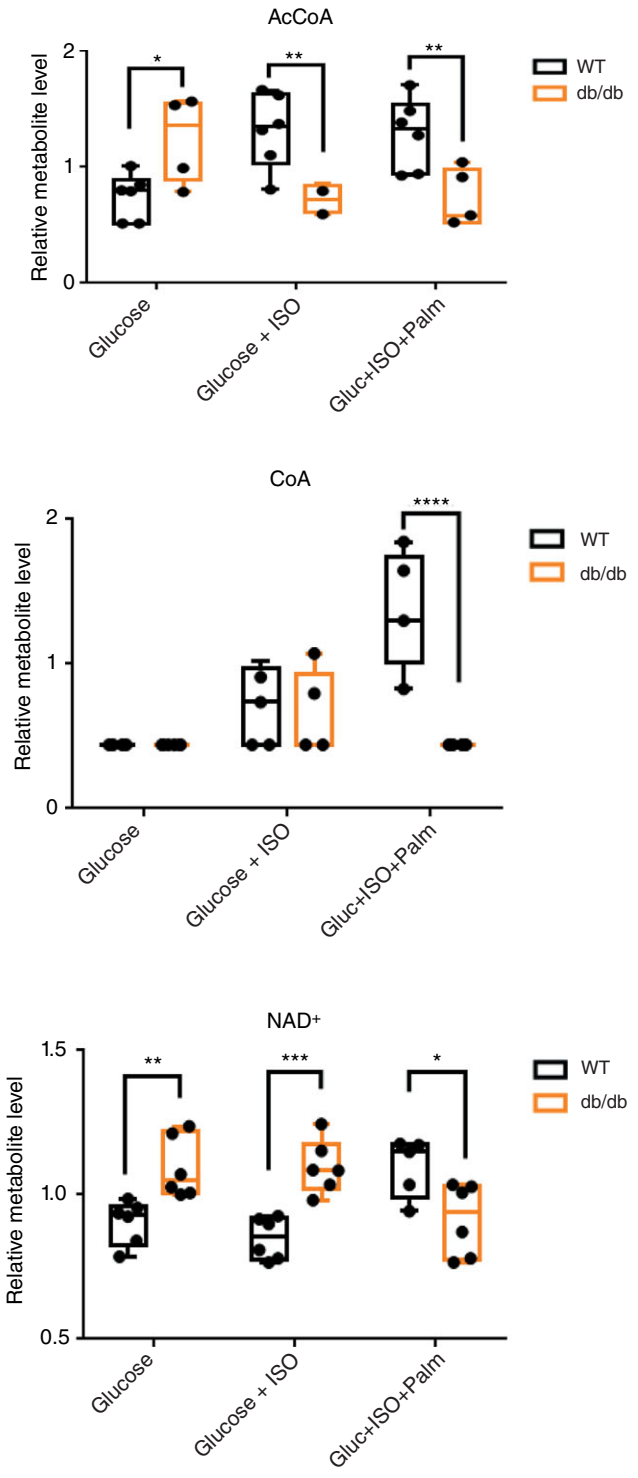

Figure 9. Two-way ANOVA of metabolites from the TCA cycle
The ratio AcCoA/CoA, a main regulator of the pyruvate dehydrogenase (PDH) complex, was significantly decreased in *db/db* mouse hearts when both glucose and Palm were in the presence of adrenergic stimulation (from 2.7 in glucose to 1.12 in GIP) indicating a higher flux through PDH according to our computational model (Cortassa *et al.* 2017*b*), and in agreement with reported experimental data (Pettit *et al.* 1975). A similar effect happened in WT hearts where the AcCoA/CoA ratio decreased from 1.7 to 0.93, under the same conditions. The quantitative assessment of metabolites concentration is shown in Tables 3 and 4 (see Methods for details). $^{*}P < 0.05$; $^{**}P < 0.01$; $^{***}P < 0.001$; $^{****}P < 0.0001$. [Colour figure can be viewed at wileyonlinelibrary.com]

Discussion

Our study provides new evidence supporting the notion of an extensive catabolic network remodelling in the diabetic heart, summarized in Fig. 13. The fluxome remodelling in the T2DM heart led to improved redox, both in cytoplasmic and mitochondrial compartments. When T2DM hearts were subjected to hyperglycaemic and neurohormonal stress (HG/ISO), they exhibited increased fluxes through the polyol pathway that, when Palm was added, decreased 6-fold at preserved flux through the NADPH-generating PP pathway (Fig. 12). Despite a decrease of the glycolytic flux, the presence of Palm enabled sustained flux through the PP pathway, thus helping to restore myocardial redox balance. Palm reactivated oxidative mitochondrial metabolism, i.e. β-oxidation and the TCA cycle, in T2DM hearts exposed to HG+ISO. The higher flux contribution from the 'lower' part of the TCA cycle via mitochondrial AAT in T2DM hearts (Figs 12 and 13) would also confer, in principle, a redox advantage with respect to WT. Overall, the changes elicited by FA oxidation provide a biochemical rationale to understand the improved redox balance that underlies the preserved LV (Fig. 2) and myocyte function in T2DM hearts (Tocchetti *et al.* 2012).

The causal relationship between myocardial redox improvement and enhanced contractility was previously demonstrated in two different animal models of T2DM (Tocchetti *et al.* 2012; Bhatt *et al.* 2015), and in a type 1 diabetes model in the guinea pig (Tocchetti *et al.* 2015). Essentially, it was found that restoration of redox balance is the underlying common mediator of enhanced contractile and Ca^{2+} handling performance, independently promoted by Palm or glutathione ethyl ester (a cell-permeant form of glutathione), under high glucose at the level of the cardiomyocyte, cardiac trabeculae or intact heart (Tocchetti *et al.* 2012, 2015; Aon *et al.* 2015; Bhatt *et al.* 2015).

The T2DM condition elicits a major redistribution of fluxes through glucose and redox-related pathways

The ~2-fold and ~3-fold lower fluxes through glycolysis and glycogenolysis, respectively, along with the 5-fold higher flux through the polyol pathway, in the T2DM compared to the WT heart (Figs 12 and 13), imply a different baseline enzymatic/kinetic make-up for diabetic mice as suggested by V_{max} values, which, in turn, determine the fluxome remodelling. It is likely that these differences are due to the insulin-resistant phenotype of *db/db* mice, which may affect storage of glycogen, or

its degradation via effects on β-adrenergic stimulation. Myocardial glycogenolysis is a physiological response to adrenergic stimulation (Goodwin *et al.* 1998*a*; McConville *et al.* 2007). Although 3-fold smaller in the T2DM mouse heart than in WT heart, glycogenolysis appears to be quantitatively relevant under all conditions tested herein, including β-adrenergic stimulation (Fig. 12). Other mechanisms influencing the kinetic make-up of diabetic mice could be mediated by post-translational modifications such as acetylation and palmitoylation (Vadvalkar *et al.* 2013; Abo Alrob & Lopaschuk, 2014; Reilly *et al.* 2015; Al Batran & Ussher, 2017). Similar molecular mechanisms may apply to the above-mentioned differential function of the TCA cycle via AAT between *db*/*db* and WT mice (Fig. 12).

Several metabolites from the methionine cycle and transsulfuration pathway, which leads to the synthesis of glutathione (Mato *et al.* 1997), were present at higher levels in the heart from diabetic mice (Fig. 10). However, the levels of GSH and GSSG were significantly decreased under all treatment conditions (G, GI, GIP) in the heart from diabetic *vs.* WT mice (Fig. 10). The lower levels of GSH/GSSG exhibited by the diabetic heart were concomitant with the significantly higher levels of methionine sulfoxide, a biomarker of oxidative stress (Fig. 10). In the same vein, the increased level of

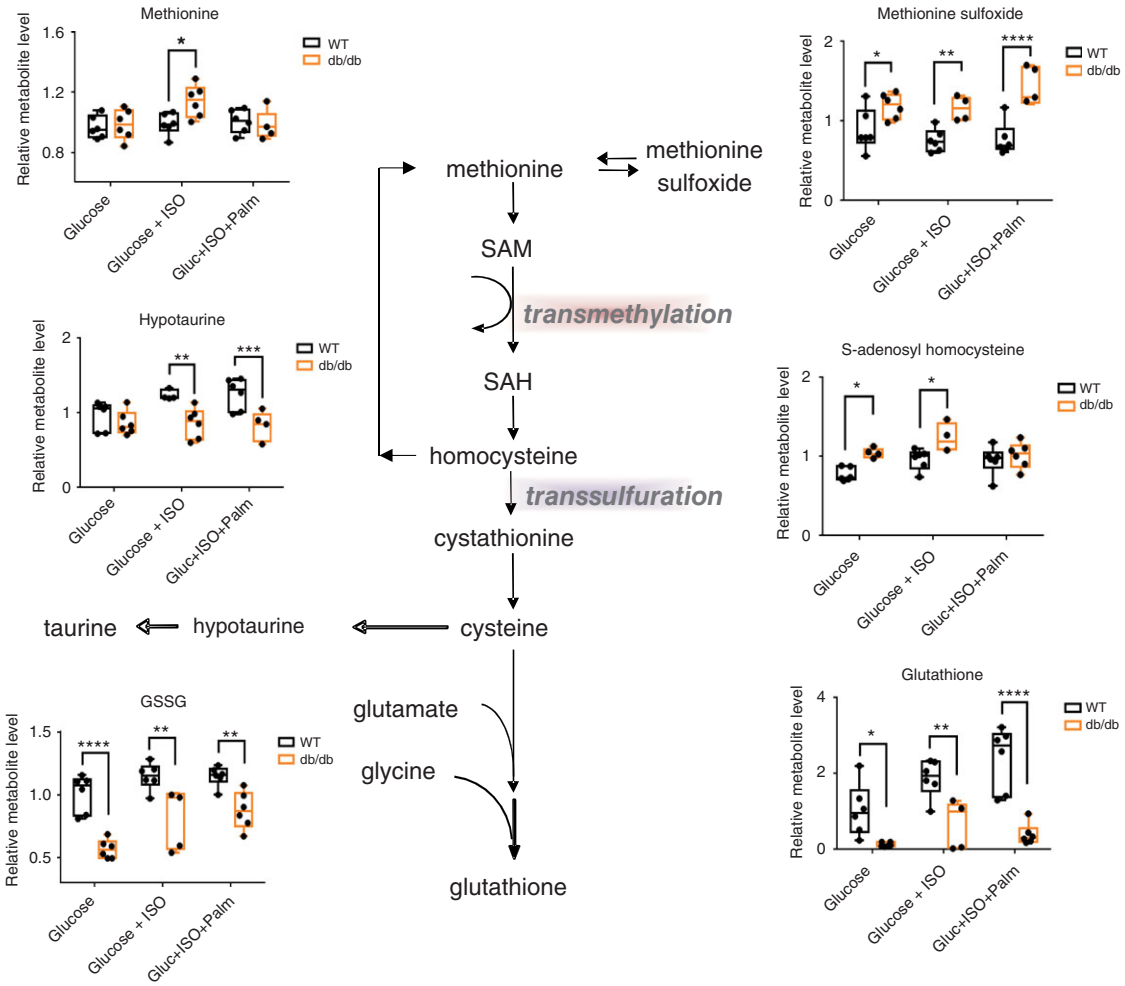

Figure 10. Redox-related pathways and oxidative stress in the *db*/*db* heart
The methionine cycle and the transsulfuration pathway to glutathione are depicted. Several metabolites such as methionine, methionine sulfoxide and *S*-adenosyl homocysteine (SAH), involved in the methionine cycle and the transsulfuration pathway leading to the synthesis of glutathione, were present in the profiles and significantly elevated in the hearts from diabetic compared to WT mice. The methylation cycle involves the conversion of methionine, via *S*-adenosylmethionine (SAM) and *S*-adenosylhomocysteine (SAHC), into homocysteine, followed by reconversion of homocysteine into methionine. To operate the methylation cycle *in vivo*, homocysteine and adenosine should be removed rapidly. Homocysteine is converted into cystathionine and its derivatives (cysteine, GSH, taurine, inorganic sulfate) by the transsulfuration pathway, or used again for the resynthesis of methionine (Mato *et al.* 1997). [Colour figure can be viewed at wileyonlinelibrary.com]

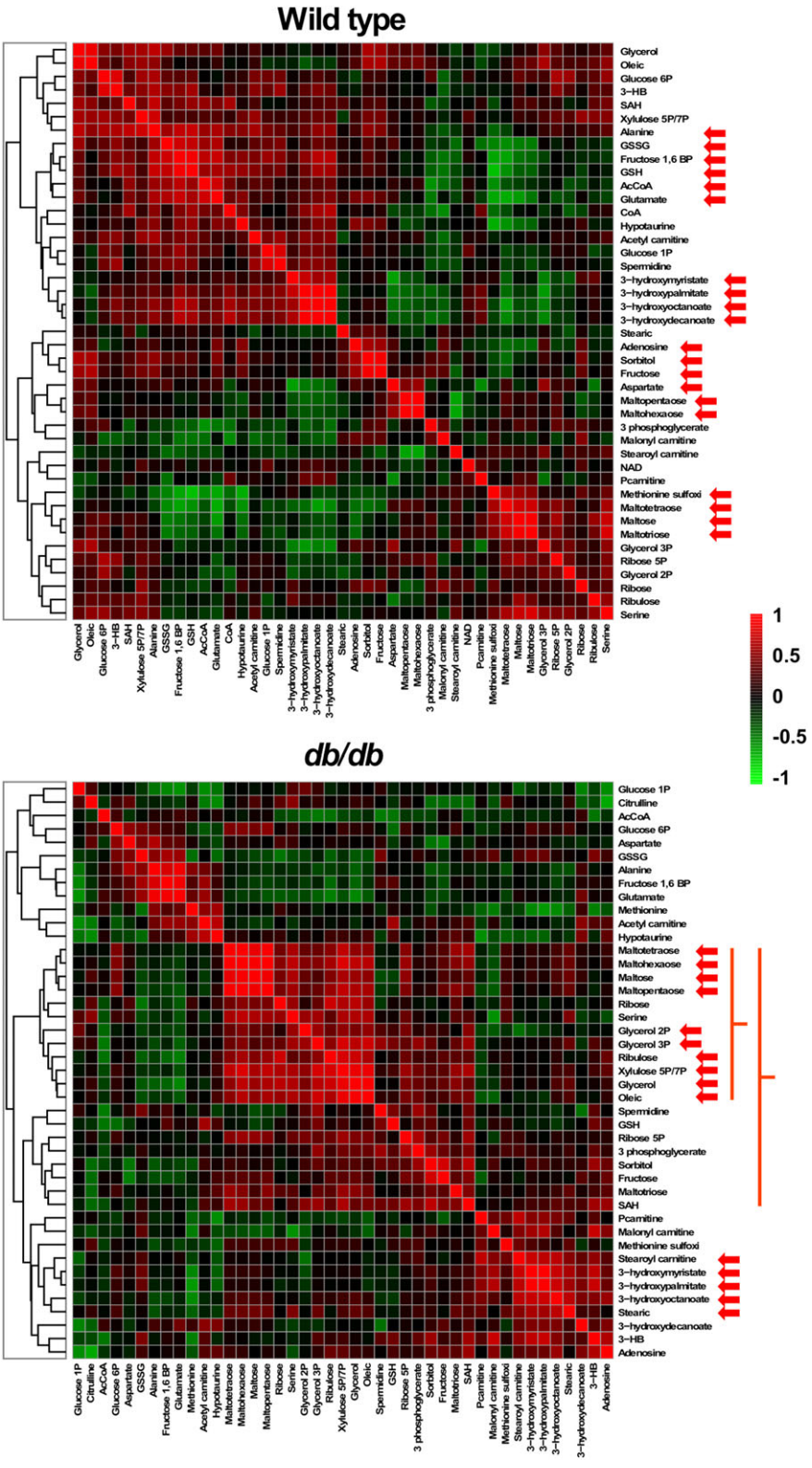

Figure 11. Correlation matrix of metabolite profiles from WT or *db*/*db* heart obtained under G, GI and GIP conditions

Correlation matrix of the 43 metabolites responsible for treatment separations under G, GI and GIP conditions in hearts from WT or diabetic mice was obtained using MetaboAnalyst 3.0 (Xia & Wishart, 2016). The type (positive or negative) and strength (colour intensity) of correlation are coded red and green, respectively, according to the bar on the right, and normalized between 1 and −1. Red arrows on the left denote strong positively correlated metabolites. Red on the diagonal correspond to correlation 1 for each metabolite with respect to itself. Because each group is correlated against itself, the clustering, and thus the order of metabolites, is not the same in WT and diabetic metabolomes. GSH, reduced glutathione; GSSG, oxidized glutathione; 3-HB, 3-hydroxybutyrate; SAH, S-adenosylhomocysteine.

Table 3. Comparison of experimental and model-simulated metabolite concentrations obtained from hearts of diabetic (*db*/*db*) mice

	G		GI		GIP	
Metabolite	Experimental	Model	Experimental	Model	Experimental	Model
Glucose(ex)	30		30		30	
Glucose(in)	5.5	5.37	5.42	4.94	0.32	0.337
G1P	0.135 ± 0.015	0.195	0.153 ± 0.008	0.149	0.146 ± 0.016	0.180
F6P + G6P	3.71 ± 0.48	3.23	3.75 ± 0.26	2.48	3.55 ± 0.31	2.98
F1,6BP	0.049 ± 0.012	0.060	0.015 ± 0.004	0.035	0.011 ± 0.002	0.012
G3P	<0.01	4.9×10^{-3}	<0.01	6.8×10^{-3}	<0.01	3.4×10^{-3}
1,3BPG	<0.01	1.7×10^{-4}	<0.01	2.6×10^{-4}	<0.01	1.2×10^{-4}
3PG	0.504 ± 0.022	0.146	0.64 ± 0.07	0.356	0.62 ± 0.05	0.087
PEP	<0.01	1.8×10^{-3}	<0.01	7.4×10^{-4}	<0.01	9.2×10^{-4}
Pyruvate	<0.01	4.8×10^{-3}	<0.01	4.96×10^{-3}	<0.01	3.9×10^{-3}
Ru5P + X5P	4.2 ± 0.5	2.06	4.4 ± 0.4	2.20	3.7 ± 0.4	2.41
R5P	0.48 ± 0.04	0.87	0.38 ± 0.03	0.93	0.35 ± 0.04	1.02
Xylitol	0.9 ± 0.12	0.429	0.81 ± 0.07	0.473	0.804 ± 0.06	0.550
Sorbitol	1.2 ± 0.1	1.51	1.1 ± 0.3	1.36	1.5 ± 0.2	1.26
Fructose	4.0 ± 0.4	2.57	2.5 ± 0.5	2.24	3.2 ± 0.5	2.28
AcCoA*	1.94 ± 0.74	1.42	1.74± 0.79	1.40	1.56± 0.88	1.41
Succ	0.12 ± 0.02	0.102	0.11 ± 0.05	0.09	0.102 ± 0.023	0.10
Fum	1.86 ± 1.01	1.59	1.69 ± 0.53	1.52	1.55 ± 0.55	1.57
Iso	<0.01	0.014	<0.01	0.014	<0.01	0.014
αKG	<0.01	0.004	<0.01	0.0037	<0.01	0.0039

Experimental and model-simulated concentrations are expressed in mmol L^{-1}, and experimental values are displayed as mean ± SEM ($n = 6$). *AcCoA concentration is given in μmol L^{-1}. G, 30 mM glucose; GI, G + 10 nM ISO; GIP, G + I + 0.4 mM Palm. 1,3BPG, 1,3-bisphosphoglycerate; 3PG, 3-phosphoglycerate; AcCoA, acetyl-CoA; αKG, α-ketoglutarate; F1,6BP, fructose 1,6-bisphosphate; F6P, fructose 6-phosphate; Fum, fumarate; Glucose(ex), extracellular glucose; Glucose(in), intracellular glucose; G1P, glucose 1-phosphate; G3P, glyceraldehyde 3-phosphate; G6P, glucose 6-phosphate; Iso, isocitrate; PEP, phosphoenolpyruvate; R5P, ribose 5-phosphate; Ru5P, ribulose 5-phosphate; Succ, succinate; X5P, xylulose 5-phosphate.

methionine sulfoxide is also in agreement with the more oxidized cardiac redox status of the *db*/*db* hearts (Tocchetti *et al.* 2012; Aon & Foster, 2015; Aon *et al.* 2015) because methionine can function as an antioxidant and, therefore, can be readily oxidized to methionine sulfoxide by ROS (Levine *et al.* 2000). Using two-photon laser scanning fluorescence microscopy, previous data obtained in *db*/*db* cardiomyocytes showed decreased GSH levels along with increased oxidative stress (Tocchetti *et al.* 2012). Adding cell-perment GSH ethyl ester to *db*/*db* cardiac myocytes increased their intracellular pool of GSH and decreased oxidative stress while improving contractility and Ca^{2+} handling (Tocchetti *et al.* 2012).

The concept that a shift in cardiac metabolism from glucose to FAs jeopardizes glucose oxidation and heart function, while increasing mitochondrial ROS emission, has been a main tenet of the pathophysiology of diabetic cardiomyopathy (Anderson *et al.* 2009; Kok & Brindley, 2012; Aon *et al.* 2015). In diabetes, sympathetic adrenergic overdrive represents a risk factor (Jouven *et al.* 2005; Thackeray *et al.* 2012) by further exacerbating myocardial energy demand and oxidative stress (Aon *et al.* 2009; Xie *et al.* 2013). Here, we document that, in T2DM hearts, exogenous Palm, under stressful HG/ISO conditions, elicits a beneficial 17-fold fall in intracellular glucose concentration (Table 3) with respect to hyperglycaemic conditions without Palm. Existing evidence supports a role for Palm in reducing glucose uptake acutely via effects on the translocation of GLUT1 and GLUT4 in perfused rat heart (Wheeler *et al.* 1994).

The possible function of the glycerol-3P/glycerol cycle in shunting glycerol away from triglyceride degradation into glycolysis is an additional insight provided by bioinformatic analysis regarding the metabolic impact of diabetes in the *db*/*db* heart phenotype (Figs 4 and 5). The glycerol-3P/glycerol cycle is considered an important process for the balance of glucose and lipid metabolism as well as maintenance of energy homeostasis (Zechner *et al.* 2012; Possik *et al.* 2017). Phosphoglycolate phosphatase can catalyse the conversion of glycerol-3P into glycerol (Possik *et al.* 2017). Overexpression of this enzyme in cells produced an increase in glycerol release, whereas lipogenesis and triglycerides were decreased, and FA release elevated (Mugabo *et al.* 2016). These results suggest that a glycerol-3P shunt to glycolysis could represent a positive mechanism of substrate selection towards glucose while degrading triglycerides and reducing fat storage.

Table 4. Comparison of experimental and model-simulated metabolite concentrations obtained from hearts of wild-type (WT) mice

	G		GI		GIP	
Metabolite	Experimental	Model	Experimental	Model	Experimental	Model
Glucose(ex)	11		11		11	
Glucose(in)	1.52	1.43	1.91	2.28	1.48	1.77
G1P	0.163 ± 0.004	0.059	0.192 ± 0.013	0.082	0.206 ± 0.017	0.09
F6P + G6P	4.04 ± 0.97	0.9	4.8 ± 0.4	1.349	5.17 ± 0.39	1.477
F1,6BP	0.015 ± 0.005	0.016	0.021 ± 0.002	0.0205	0.026 ± 0.002	0.0208
G3P	<0.01	0.008	<0.01	0.001	<0.01	0.001
1,3BPG	<0.01	2.6×10^{-4}	<0.01	3.6×10^{-4}	<0.01	4.4×10^{-4}
3-PG	0.57 ± 0.04	0.74	0.47 ± 0.02	0.3212	0.44 ± 0.03	0.4681
PEP	<0.01	1.4×10^{-4}	<0.01	1.3×10^{-4}	<0.01	1.4×10^{-4}
Pyruvate	<0.01	3.8×10^{-4}	<0.01	3.7×10^{-4}	<0.01	3.8×10^{-4}
Ru5P + X5P	2.58 ± 0.68	2.93	3.2 ± 0.4	3.18	3.33 ± 0.02	3.19
R5P	0.29 ± 0.07	1.2	0.29 ± 0.04	1.35	0.26 ± 0.02	1.36
Xylitol	0.65 ± 0.18	0.71	0.79 ± 0.07	0.81	0.51 ± 0.05	0.74
Sorbitol	0.67 ± 0.32	0.63	0.68 ± 0.17	0.49	0.56 ± 0.11	0.42
Fructose	1.7 ± 1.2	1.72	1.4 ± 0.3	1.47	1.2 ± 0.2	1.26
AcCoA*	1.49 ± 0.17	1.23	2.27± 0.56	2.05	2.22± 0.53	2.10
Succ	0.103 ± 0.021	0.143	0.121 ± 0.014	0.114	0.126 ± 0.027	0.124
Fum	1.43 ± 0.91	1.87	1.88 ± 0.89	1.65	1.62 ± 0.54	1.73
Iso	<0.01	0.0035	<0.01	0.0031	<0.01	0.0035
αKG	<0.01	0.0052	<0.01	0.0042	<0.01	0.0045

Experimental and model-simulated concentrations are expressed in mmol L^{-1}, and experimental values are displayed as mean ± SEM ($n = 6$). *AcCoA concentration is given in μmol L^{-1}. G, 11 mM glucose; GI, G + 10 nM ISO; GIP, G + I + 0.2 mM Palm. For abbreviations, see Table 3.

Mitochondrial redox remodelling in T2DM

Mitochondria play a prominent role as a source of oxidative stress in the T2DM mouse heart (Stanley *et al.* 2011; Aon *et al.* 2012), thus further underscoring the relevance of the PP pathway flux activity, as an NADPH provider for the regeneration of antioxidant defences. The key role played by the PP pathway in cardiomyocyte function has been highlighted before (Hecker *et al.* 2013*a*). G6PD is critical for maintenance of cytoplasmic redox status in adult cardiomyocytes, and its deficiency may lead to contractile dysfunction (Jain *et al.* 2003).

Regarding FA oxidation, multivariate (heat map) (Fig. 4) and univariate (two-way ANOVA) statistics (Figs 8 and 9) together with fluxomics (Fig. 12) support the idea of enhanced flux through β-oxidation and the TCA cycle in the presence of Palm (Fig. 13). Although expected, it is remarkable that, under this condition, the flux of pyruvate supplied from glucose catabolism contributes to a significant extent to the pool of AcCoA relative to Palm oxidation, 41 *vs.* 33.6 μM s^{-1}, respectively (Fig. 12; the flux from palmitoyl CoA, C_{16}CoA, $4.2 \times 8 = 33.6$). These results suggest that, under the conditions of this study, the initial enzymatic and hence the kinetic make-up of the diabetic mice exerts a considerable influence on the substrate selection and flux distribution through central catabolism. Palmitate's presence improves redox status, favouring the remodelling of the heart's fluxome from diabetic mice (Figs 12 and 13), concomitantly with preserved coronary vasodilation and enhanced contractile performance (Fig. 2).

Limitations of this study

In the present work, we have compared WT and *db*/*db* hearts under conditions mimicking their respective circulation levels of glucose and Palm. Controls exposing WT and diabetic hearts to reverse substrate conditions, i.e. WT to high glucose/Palm, and diabetic to low glucose/Palm, were not included in this study, thus precluding a clear distinction of the effects due to substrate *vs.* genotype. It should be noted, however, that these controls were included in our previous work in another leptin receptor-deficient T2DM animal model, the Zucker diabetic fatty (ZDF) rat. Cardiac trabeculae from ZDF and lean control rats were studied under working (i.e. loaded) conditions. The results showed that from the energetic (respiration) and functional (contractility) standpoints measured simultaneously, euglycaemia or hyperglycaemia (without palmitate) produced outputs that were not significantly different between lean control and ZDF rats. Moreover, euglycaemia with palmitate also produced similar results in both groups. The main differences in contractile/energetic activities between lean and ZDF

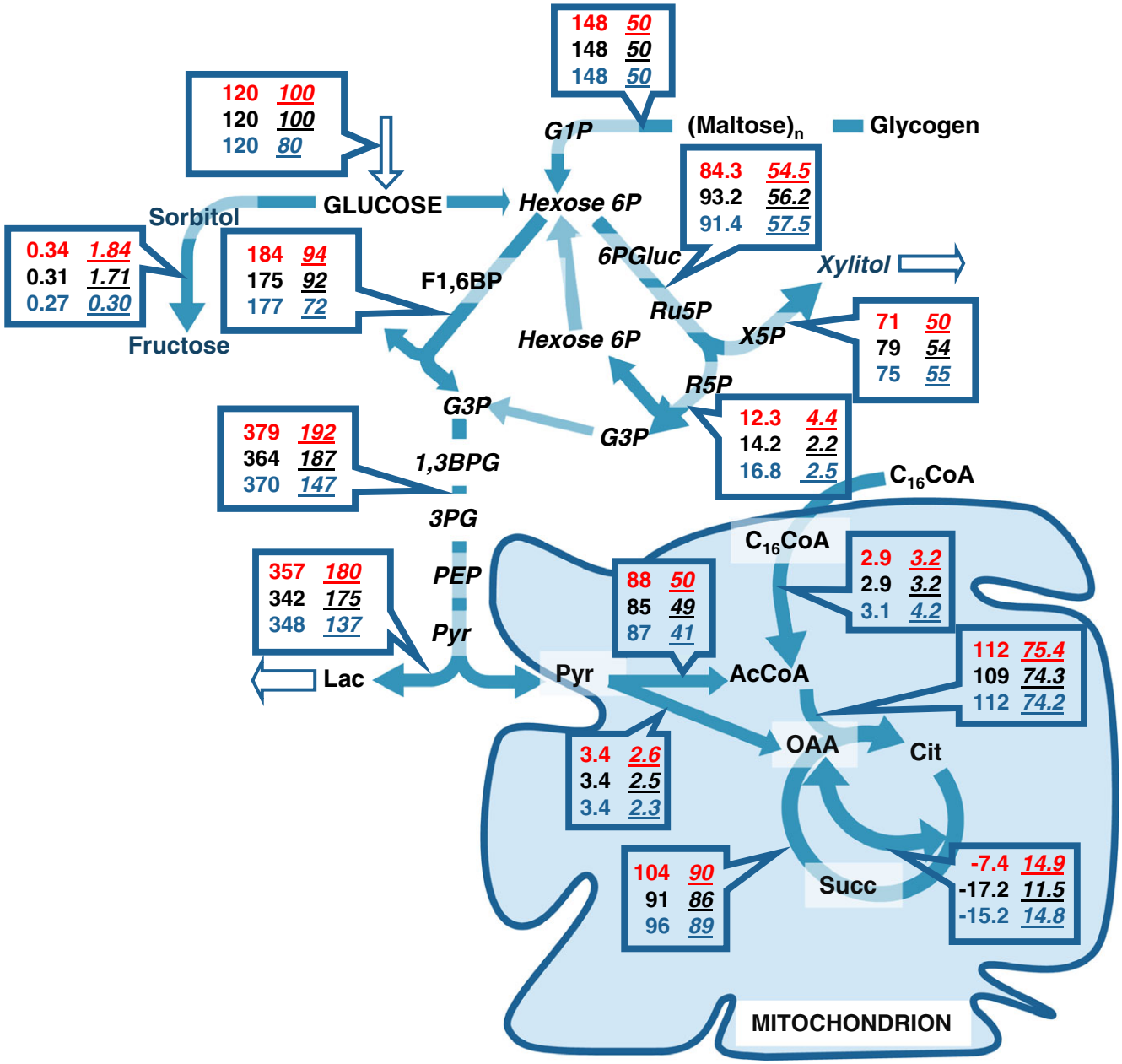

Figure 12. Fluxome remodelling and flux distribution in central catabolism from WT and diabetic mouse hearts
Depicted are the fluxes (in μM s^{-1}) sustained by the pathways involved in glucose and FA utilization. Metabolite concentrations (in mM) were determined as described in Methods and used as inputs for the calculation of fluxes (in μM s^{-1}, equivalent to nmol s^{-1} mL^{-1} intracellular water) sustained by the pathways involved in glucose and FA utilization in cytoplasmic and mitochondrial compartments (see legend to Fig. 1). For flux calculation we used our computational model of central catabolism, which was validated by its ability to reproduce the metabolite concentrations determined experimentally (Tables 3 and 4), after metabolite profiling of WT and T2DM hearts perfused under the conditions described in the legend of Fig. 2. Boxed are the flux values corresponding to WT and diabetic hearts (left and right, underlined, number columns, respectively) next to their respective steps in the network. Within each box, the experimental condition G, GI or GIP is denoted by a distinct colour (red, black, blue, respectively). For abbreviations, see legend to Fig. 1.

happened when working heart trabeculae were perfused in the presence of both hyperglycaemia and palmitate, with the result being detrimental for lean control and beneficial for T2DM animals (Bhatt *et al.* 2015). Therefore, a comparison under these conditions would have been unphysiological for lean controls. Similar results were found in WT and *db*/*db* Langendorff perfused hearts subjected to all substrate combinations (see Supplementary Figs. 6 and 7 in Tocchetti *et al.* 2012). Altogether, these results informed our decision to adopt the experimental design utilized in the present work.

Although *ex vivo* non-working Langendorff heart preparations are advantageous for precise control of conditions relevant for the aims of the present study, such as substrate concentrations, adrenergic stimulation (in addition to, e.g. pH, temperature, ionic composition) they are not representative of *in vivo* conditions. A main difference is given by the afterload pressure present in working heart mimicking *in vivo* function against systolic pressure. Therefore, this limitation should be considered when extrapolating the results of the present study.

Computationally, as mentioned above, our procedure generates a volume of possible model solutions because the number of unknowns (V_{max}) is larger than the individual metabolite differential equations; consequently, a unique solution cannot be determined. A potentially feasible way to improve it is to restrict the solution space by using uniform sampling Monte Carlo methods, but this is for future work. In our case, we search for the vertices of the solution space as described elsewhere (Cortassa *et al.* 2015, 2018).

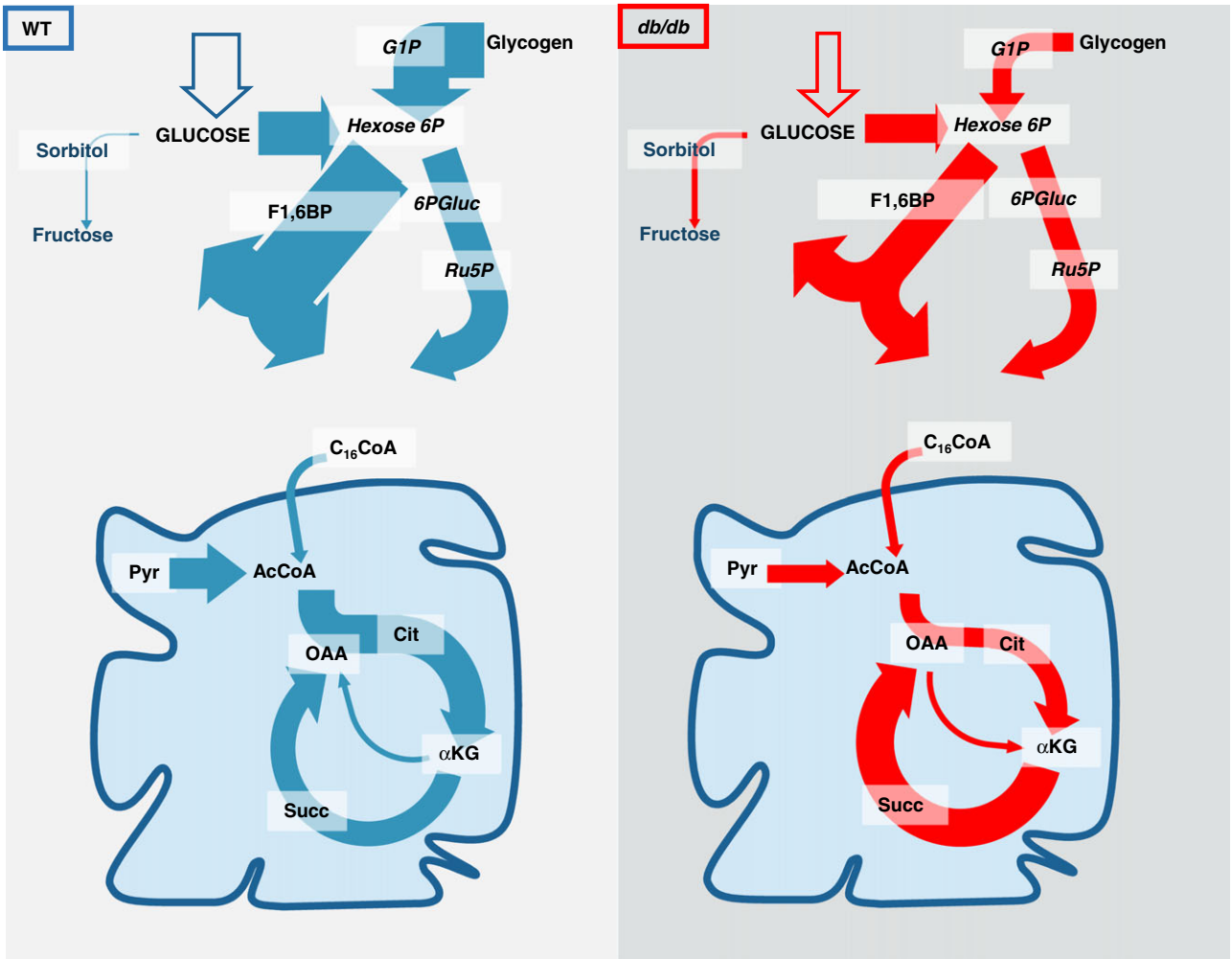

Figure 13. Schematic representation of major fluxome remodelling in central catabolism from WT and diabetic (*db*/*db*) mouse hearts
The fluxome of diabetic (right, red) and WT (left, blue) are depicted, highlighting major differences in the fluxes as denoted by arrow thickness. Fluxes throughout central catabolism were about 2-fold lower in glucose metabolism from diabetic heart. Also displayed is the higher flux through the 'lower' part of the TCA cycle in the T2DM heart, in contrast with the WT where the 'upper' part predominates. For abbreviations, see legend to Fig. 1.

Another source of uncertainty in the fluxome calculations is given by the reference fluxes that constitute the input for the optimization procedure. We did not assess reference fluxes in the intact heart, but instead measured them in isolated cardiomyocytes, which are resting cells and thus in a different physiological condition with respect to that of the myocardium in the Langendorff set-up. The fluxes derived from the isolated cardiomyocytes were then scaled up to fit those obtained from unloaded mouse hearts (Boardman *et al.* 2009). Future, in-depth work is required to validate the fluxes predicted by fluxome calculation.

Concluding remarks

Under relevant physiological conditions, related to peaks of high glucose (e.g. postprandial) and adrenergic overdrive, which impose higher work/energy demands, the initial enzymatic/kinetic make-up of diabetic mice appears to be a major determinant of quantitative differences in flux distribution. Palm-elicited fluxome remodelling helps to restore redox balance and improves T2DM heart function under stressful conditions. These findings may contribute to putting forth novel therapeutic strategies directed to preventing cardiac dysfunction and, eventually, heart failure in diabetic patients.

References

Abo Alrob O & Lopaschuk GD (2014). Role of CoA and acetyl-CoA in regulating cardiac fatty acid and glucose oxidation. *Biochem Soc Trans* **42**, 1043–1051.

Al Batran R & Ussher JR (2017). Revisiting protein acetylation and myocardial fatty acid oxidation. *Am J Physiol Heart Circ Physiol* **313**, H617–H619.

Anderson EJ, Lustig ME, Boyle KE, Woodlief TL, Kane DA, Lin CT, Price JW 3rd, Kang L, Rabinovitch PS, Szeto HH, Houmard JA, Cortright RN, Wasserman DH & Neufer PD (2009). Mitochondrial H_2O_2 emission and cellular redox state link excess fat intake to insulin resistance in both rodents and humans. *J Clin Invest* **119**, 573–581.

Aon MA, Cortassa S, Akar FG, Brown DA, Zhou L & O'Rourke B (2009). From mitochondrial dynamics to arrhythmias. *Int J Biochem Cell Biol* **41**, 1940–1948.

Aon MA & Foster DB (2015). Diabetic cardiomyopathy and the role of mitochondrial dysfunction: novel insights, mechanisms, and therapeutic strategies. *Antioxid Redox Signal* **22**, 1499–1501.

Aon MA, Stanley BA, Sivakumaran V, Kembro JM, O'Rourke B, Paolocci N & Cortassa S (2012). Glutathione/thioredoxin systems modulate mitochondrial H_2O_2 emission: an experimental-computational study. *J Gen Physiol* **139**, 479–491.

Aon MA, Tocchetti CG, Bhatt N, Paolocci N & Cortassa S (2015). Protective mechanisms of mitochondria and heart function in diabetes. *Antioxid Redox Signal* **22**, 1563–1586.

Balogun KA, Albert CJ, Ford DA, Brown RJ & Cheema SK (2013). Dietary omega-3 polyunsaturated fatty acids alter the fatty acid composition of hepatic and plasma bioactive lipids in C57BL/6 mice: a lipidomic approach. *PLoS One* **8**, e82399.

Bhatt NM, Aon MA, Tocchetti CG, Shen X, Dey S, Ramirez-Correa G, O'Rourke B, Gao WD & Cortassa S (2015). Restoring redox balance enhances contractility in heart trabeculae from type 2 diabetic rats exposed to high glucose. *Am J Physiol Heart Circ Physiol* **308**, H291–H302.

Boardman N, Hafstad AD, Larsen TS, Severson DL & Aasum E (2009). Increased O_2 cost of basal metabolism and excitation-contraction coupling in hearts from type 2 diabetic mice. *Am J Physiol Heart Circ Physiol* **296**, H1373–H1379.

Boudina S & Abel ED (2010). Diabetic cardiomyopathy, causes and effects. *Rev Endocr Metab Disord* **11**, 31–39.

Boudina S, Sena S, Theobald H, Sheng X, Wright JJ, Hu XX, Aziz S, Johnson JI, Bugger H, Zaha VG & Abel ED (2007). Mitochondrial energetics in the heart in obesity-related diabetes: direct evidence for increased uncoupled respiration and activation of uncoupling proteins. *Diabetes* **56**, 2457–2466.

Brownlee M (2001). Biochemistry and molecular cell biology of diabetic complications. *Nature* **414**, 813–820.

Causse E, Fournier P, Roncalli J, Salvayre R & Galinier M (2017). Serum allantoin and aminothiols as biomarkers of chronic heart failure. *Acta Cardiol* **72**, 397–403.

Cortassa S, Aon MA, O'Rourke B, Jacques R, Tseng HJ, Marban E & Winslow RL (2006). A computational model integrating electrophysiology, contraction, and mitochondrial bioenergetics in the ventricular myocyte. *Biophys J* **91**, 1564–1589.

Cortassa S, Caceres V, Bell LN, O'Rourke B, Paolocci N & Aon MA (2015). From metabolomics to fluxomics: a computational procedure to translate metabolite profiles into metabolic fluxes. *Biophys J* **108**, 163–172.

Cortassa S, O'Rourke B, Winslow RL & Aon MA (2009). Control and regulation of integrated mitochondrial function in metabolic and transport networks. *Int J Mol Sci* **10**, 1500–1513.

Cortassa S, Sollott SJ & Aon MA (2017*a*). Mitochondrial respiration and ROS emission during β-oxidation in the heart: An experimental-computational study. *PLoS Comput Biol* **13**, e1005588.

Cortassa S, Sollott SJ & Aon MA (2017*b*). Substrate selection and its impact on mitochondrial respiration and redox. In *Molecular Basis for Mitochondrial Signaling*, ed. Rostovtseva TK. Springer International Publishing AG.

Cortassa S, Sollott SJ & Aon MA (2018). Computational modeling of mitochondrial function from a systems biology perspective. *Methods Mol Biol* **1782**, 249–265.

Giacco F & Brownlee M (2010). Oxidative stress and diabetic complications. *Circ Res* **107**, 1058–1070.

Goh KY, Qu J, Hong H, Liu T, Dell'Italia LJ, Wu Y, O'Rourke B & Zhou L (2016). Impaired mitochondrial network excitability in failing guinea-pig cardiomyocytes. *Cardiovasc Res* **109**, 79–89.

Goodwin GW, Ahmad F, Doenst T & Taegtmeyer H (1998*a*). Energy provision from glycogen, glucose, and fatty acids on adrenergic stimulation of isolated working rat hearts. *Am J Physiol* **274**, H1239–H1247.

Goodwin GW, Taylor CS & Taegtmeyer H (1998*b*). Regulation of energy metabolism of the heart during acute increase in heart work. *J Biol Chem* **273**, 29530–29539.

Hecker PA, Leopold JA, Gupte SA, Recchia FA & Stanley WC (2013*a*). Impact of glucose-6-phosphate dehydrogenase deficiency on the pathophysiology of cardiovascular disease. *Am J Physiol Heart Circ Physiol* **304**, H491–H500.

Hecker PA, Lionetti V, Ribeiro RF Jr, Rastogi S, Brown BH, O'Connell KA, Cox JW, Shekar KC, Gamble DM, Sabbah HN, Leopold JA, Gupte SA, Recchia FA & Stanley WC (2013*b*). Glucose 6-phosphate dehydrogenase deficiency increases redox stress and moderately accelerates the development of heart failure. *Circ Heart Fail* **6**, 118–126.

Hue L & Taegtmeyer H (2009). The Randle cycle revisited: a new head for an old hat. *Am J Physiol Endocrinol Metab* **297**, E578–E591.

Jain M, Brenner DA, Cui L, Lim CC, Wang B, Pimentel DR, Koh S, Sawyer DB, Leopold JA, Handy DE, Loscalzo J, Apstein CS & Liao R (2003). Glucose-6-phosphate dehydrogenase modulates cytosolic redox status and contractile phenotype in adult cardiomyocytes. *Circ Res* **93**, e9–e16.

Jouven X, Empana JP, Schwartz PJ, Desnos M, Courbon D & Ducimetiere P (2005). Heart-rate profile during exercise as a predictor of sudden death. *N Engl J Med* **352**, 1951–1958.

Kashiwaya Y, Sato K, Tsuchiya N, Thomas S, Fell DA, Veech RL & Passonneau JV (1994). Control of glucose utilization in working perfused rat heart. *J Biol Chem* **269**, 25502–25514.

Kembro JM, Aon MA, Winslow RL, O'Rourke B & Cortassa S (2013). Integrating mitochondrial energetics, redox and ROS metabolic networks: A two-compartment model. *Biophys J* **104**, 332–343.

Kok BP & Brindley DN (2012). Myocardial fatty acid metabolism and lipotoxicity in the setting of insulin resistance. *Heart Fail Clin* **8**, 643–661.

Kurz FT, Kembro JM, Flesia AG, Armoundas AA, Cortassa S, Aon MA & Lloyd D (2017). Network dynamics: quantitative analysis of complex behavior in metabolism, organelles, and cells, from experiments to models and back. *Wiley Interdiscip Rev Syst Biol Med* **9**, https://doi.org/10.1002/wsbm.1352.

Levine RL, Moskovitz J & Stadtman ER (2000). Oxidation of methionine in proteins: roles in antioxidant defense and cellular regulation. *IUBMB Life* **50**, 301–307.

Mato JM, Alvarez L, Ortiz P & Pajares MA (1997). *S*-adenosylmethionine synthesis: molecular mechanisms and clinical implications. *Pharmacol Ther* **73**, 265–280.

McConville P, Lakatta EG & Spencer RG (2007). Greater glycogen utilization during 1- than 2-adrenergic receptor stimulation in the isolated perfused rat heart. *Am J Physiol Endocrinol Metab* **293**, E1828–E1835.

Mitchell SJ, Bernier M, Aon MA, Cortassa S, Kim EY, Fang EF, Palacios HH, Ali A, Navas-Enamorado I, Di Francesco A, Kaiser TA, Waltz TB, Zhang N, Ellis JL, Elliott PJ, Frederick DW, Bohr VA, Schmidt MS, Brenner C, Sinclair DA, Sauve AA, Baur JA & de Cabo R (2018). Nicotinamide improves aspects of healthspan, but not lifespan, in mice. *Cell Metab* **27**, 667–676.e4.

Mitchell SJ, Madrigal-Matute J, Scheibye-Knudsen M, Fang E, Aon M, Gonzalez-Reyes JA, Cortassa S, Kaushik S, Gonzalez-Freire M, Patel B, Wahl D, Ali A, Calvo-Rubio M, Buron MI, Guiterrez V, Ward TM, Palacios HH, Cai H, Frederick DW, Hine C, Broeskamp F, Habering L, Dawson J, Beasley TM, Wan J, Ikeno Y, Hubbard G, Becker KG, Zhang Y, Bohr VA, Longo DL, Navas P, Ferrucci L, Sinclair DA, Cohen P, Egan JM, Mitchell JR, Baur JA, Allison DB, Anson RM, Villalba JM, Madeo F, Cuervo AM, Pearson KJ, Ingram DK, Bernier M & de Cabo R (2016). Effects of sex, strain, and energy intake on hallmarks of aging in mice. *Cell Metab* **23**, 1093–1112.

Mugabo Y, Zhao S, Seifried A, Gezzar S, Al-Mass A, Zhang D, Lamontagne J, Attane C, Poursharifi P, Iglesias J, Joly E, Peyot ML, Gohla A, Madiraju SR & Prentki M (2016). Identification of a mammalian glycerol-3-phosphate phosphatase: Role in metabolism and signaling in pancreatic beta-cells and hepatocytes. *Proc Natl Acad Sci U S A* **113**, E430–E439.

Nakano S, Ishii I, Shinmura K, Tamaki K, Hishiki T, Akahoshi N, Ida T, Nakanishi T, Kamata S, Kumagai Y, Akaike T, Fukuda K, Sano M & Suematsu M (2015). Hyperhomocysteinemia abrogates fasting-induced cardioprotection against ischemia/reperfusion by limiting bioavailability of hydrogen sulfide anions. *J Mol Med (Berl)* **93**, 879–889.

Pettit FH, Pelley JW & Reed LJ (1975). Regulation of pyruvate dehydrogenase kinase and phosphatase by acetyl-CoA/CoA and NADH/NAD ratios. *Biochem Biophys Res Commun* **65**, 575–582.

Possik E, Madiraju SRM & Prentki M (2017). Glycerol-3-phosphate phosphatase/PGP: Role in intermediary metabolism and target for cardiometabolic diseases. *Biochimie* **143**, 18–28.

Randle PJ, Garland PB, Hales CN & Newsholme EA (1963). The glucose fatty-acid cycle. Its role in insulin sensitivity and the metabolic disturbances of diabetes mellitus. *Lancet* **1**, 785–789.

Reilly L, Howie J, Wypijewski K, Ashford ML, Hilgemann DW & Fuller W (2015). Palmitoylation of the Na/Ca exchanger cytoplasmic loop controls its inactivation and internalization during stress signaling. *FASEB J* **29**, 4532–4543.

Stanley BA, Sivakumaran V, Shi S, McDonald I, Lloyd D, Watson WH, Aon MA & Paolocci N (2011). Thioredoxin reductase-2 is essential for keeping low levels of H_2O_2 emission from isolated heart mitochondria. *J Biol Chem* **286**, 33669–33677.

Thackeray JT, Beanlands RS & Dasilva JN (2012). Altered sympathetic nervous system signaling in the diabetic heart: emerging targets for molecular imaging. *Am J Nucl Med Mol Imaging* **2**, 314–334.

Tocchetti CG, Caceres V, Stanley BA, Xie C, Shi S, Watson WH, O'Rourke B, Spadari-Bratfisch RC, Cortassa S, Akar FG, Paolocci N & Aon MA (2012). GSH or palmitate preserves mitochondrial energetic/redox balance, preventing mechanical dysfunction in metabolically challenged myocytes/hearts from type 2 diabetic mice. *Diabetes* **61**, 3094–3105.

Tocchetti CG, Stanley BA, Sivakumaran V, Bedja D, O'Rourke B, Paolocci N, Cortassa S & Aon MA (2015). Impaired mitochondrial energy supply coupled to increased H_2O_2 emission under energy/redox stress leads to myocardial dysfunction during Type I diabetes. *Clin Sci (Lond)* **129**, 561–574.

Vadvalkar SS, Baily CN, Matsuzaki S, West M, Tesiram YA & Humphries KM (2013). Metabolic inflexibility and protein lysine acetylation in heart mitochondria of a chronic model of type 1 diabetes. *Biochem J* **449**, 253–261.

Vikramadithyan RK, Hu Y, Noh HL, Liang CP, Hallam K, Tall AR, Ramasamy R & Goldberg IJ (2005). Human aldose reductase expression accelerates diabetic atherosclerosis in transgenic mice. *J Clin Invest* **115**, 2434–2443.

Wei AC, Aon MA, O'Rourke B, Winslow RL & Cortassa S (2011). Mitochondrial energetics, pH regulation, and ion dynamics: a computational-experimental approach. *Biophys J* **100**, 2894–2903.

Wheeler TJ, Fell RD & Hauck MA (1994). Translocation of two glucose transporters in heart: effects of rotenone, uncouplers, workload, palmitate, insulin and anoxia. *Biochim Biophys Acta* **1196**, 191–200.

Williamson JR, Chang K, Frangos M, Hasan KS, Ido Y, Kawamura T, Nyengaard JR, van den Enden M, Kilo C & Tilton RG (1993). Hyperglycemic pseudohypoxia and diabetic complications. *Diabetes* **42**, 801–813.

Wisneski JA, Gertz EW, Neese RA & Mayr M (1987). Myocardial metabolism of free fatty acids. Studies with ^{14}C-labeled substrates in humans. *J Clin Invest* **79**, 359–366.

Xia J, Sinelnikov IV, Han B & Wishart DS (2015). MetaboAnalyst 3.0—making metabolomics more meaningful. *Nucleic Acids Res* **43**, W251–W257.

Xia J & Wishart DS (2011). Web-based inference of biological patterns, functions and pathways from metabolomic data using MetaboAnalyst. *Nat Protoc* **6**, 743–760.

Xia J & Wishart DS (2016). Using MetaboAnalyst 3.0 for comprehensive metabolomics data analysis. *Curr Protoc Bioinformatics* **55**, 14.10.1–14.10.91.

Xie C, Biary N, Tocchetti CG, Aon MA, Paolocci N, Kauffman J & Akar FG (2013). Glutathione oxidation unmasks proarrhythmic vulnerability of chronically hyperglycemic guinea pigs. *Am J Physiol Heart Circ Physiol* **304**, H916–H926.

Zechner R, Zimmermann R, Eichmann TO, Kohlwein SD, Haemmerle G, Lass A & Madeo F (2012). FAT SIGNALS – lipases and lipolysis in lipid metabolism and signaling. *Cell Metab* **15**, 279–291.

Zhou L, Cortassa S, Wei AC, Aon MA, Winslow RL & O'Rourke B (2009). Modeling cardiac action potential shortening driven by oxidative stress-induced mitochondrial oscillations in guinea pig cardiomyocytes. *Biophys J* **97**, 1843–1852.

Zhou L, Solhjoo S, Millare B, Plank G, Abraham MR, Cortassa S, Trayanova N & O'Rourke B (2014). Effects of regional mitochondrial depolarization on electrical propagation: implications for arrhythmogenesis. *Circ Arrhythm Electrophysiol* **7**, 143–151.

Additional information

Competing interests

The authors declare that they have no competing interests.

Author contributions

The abstract and partial forms of this work have been presented at the Biophysical Society meeting in Philadelphia, PA, in February 2013, at the Keystone Meeting in Keystone, CO, in February 2013, and the Biophysical Society meetings in Baltimore, MD, in February 2014, in New Orleans, LA, February 2017, and in San Francisco, CA, February 2018.

M.A.A. and S.C. conceived the project. V.C., C.G.T., S.C., N.P. and M.A.A. ran the experiments. M.A.A., N.P., V.C., C.G.T. and S.C. assembled and interpreted input data. S.C. designed and implemented the analytical methods, wrote the code and ran the model simulations. M.A.A. performed the bioinformatic analysis. M.A.A., S.J.S. N.P. and S.C. wrote the manuscript. S.J.S., M.B., R.dC. and N.P. edited the manuscript. All authors have read and approved the final version of this manuscript and agree to be accountable for all aspects of the work in ensuring that questions related to the accuracy or integrity of any part of the work are appropriately investigated and resolved. All persons designated as authors qualify for authorship, and all those who qualify for authorship are listed.

Funding

This work was supported by the Intramural Research Program of the NIA/NIH, and NIH grants R01-HL091923-01 (M.A.A., N.P.), and R21HL106054 (S.C.).

Supporting information

Additional supporting information may be found online in the Supporting Information section at the end of the article.

Supplementary Table S1. Parameter values used in the glycolysis rate expressions
Supplementary Table S2. Parameter values used in the glycogenolysis, pentose phosphate and polyol pathway rate expressions
Supplementary Table S3. Parameter values of mitochondrial energy metabolism and β-oxidation rate equations
Supplementary Table S4. Parameter values of mitochondrial Calcium and substrates transport rate equations